Analysis and Parametric Identification of Air Foil Bearing Rotor System

Thesis submitted to the

National Institute of Technology Rourkela

in partial fulfillment of the requirements

for the degree of

Master of Technology

in

Mechanical Engineering

(Specialization – Machine Design and Analysis)

by

Rahul Singh

(Roll Number: 214ME1304)

Under the supervision of

Prof. J. Srinivas

May 2016

Department of Mechanical Engineering
National Institute of Technology Rourkela

Mechanical Engineering
National Institute of Technology Rourkela

J. Srinivas
Associate Professor

May 23, 2016

Supervisor's Certificate

This is to certify that the work presented in this dissertation entitled "***Analysis and parametric identification of air foil bearing rotor system***" by **''*RAHUL SINGH*''**, Roll Number **214ME1304**, is a record of original research carried out by him under my supervision and guidance in partial fulfillment of the requirements for the degree of ***Master of Technology*** **in** ***Mechanical Engineering***. Neither this dissertation nor any part of it has been submitted for any degree or diploma to any institute or university in India or abroad.

J. Srinivas

Dedicated to My Parents

Declaration of Originality

I, **RAHUL SINGH**, Roll Number **214ME1304** hereby declare that this thesis entitled "***Analysis and parametric identification of air foil bearing rotor system* "** represents my original work carried out as a master student of NIT Rourkela and, to the best of my knowledge, it contains no material previously published or written by another person, nor any material presented for the award of any other degree or diploma of NIT Rourkela or any other institution. Any contribution made to this research by others, with whom I have worked at NIT Rourkela or elsewhere, is explicitly acknowledged in the dissertation. Works of other authors cited in this dissertation have been duly acknowledged under the section "Bibliography". I have also submitted my original research records to the scrutiny committee for evaluation of my dissertation.

MAY 23, 2016

Rahul Singh

NIT Rourkela

Acknowledgment

The research reported here has been carried out in the **Department of Mechanical Engineering, National Institute of Technology Rourkela.** I am greatly indebted to many persons for helping me complete this dissertation.

First and foremost, I would like to express my sense of gratitude and indebtedness to my supervisor **Prof. J. Srinivas,** Assistant Professors in the Department of Mechanical Engineering, for their inspiring guidance, encouragement, and untiring effort throughout the course of this work. Their timely help and painstaking efforts made it possible to present the work contained in this thesis. I consider myself fortunate to have worked under their guidance. Also, I am indebted to them for providing all official and laboratory facilities.

I am grateful to Director, **Prof. S.K. Sarangi** and **Prof. S.S. Mahapatra**, Head of Mechanical Engineering Department, National Institute of Technology, Rourkela, for their kind support and concern regarding my academic requirements.

MAY 23, 2016
NIT Rourkela

Rahul Singh
Roll Number: 214ME1304

Abstract

With the increasing demand for high speed turbomachinery, the dynamic analysis of rotor bearing system has become very important. Foil bearings with their exceptional feature of negligible wear has gained a very important place in the field of turbomachinery but the nonlinearities present in the bearing call for the dynamic analysis of these bearings. In the present work, a dynamic modeling approach and parametric identification scheme of a single disc rotor mounted on foil bearings is presented. Rotor is analyzed with conventional lumped parameter model. The time varying bearing forces are obtained by solving compressible Reynold's equation using finite difference scheme and the convergence is checked using Gauss Sidle method. Effects of number of bump foils, foil thickness and bump pitch at different speeds of operation of rotor are studied on the dynamic response of rotor. For solving dynamic equations, Newmark method is employed using Matlab. A solid model of the rotor is prepared and then it is analyzed to obtain various critical speeds of the system and to obtain mode shapes at those speeds. A generalized model is developed based on radial basis neural networks to predict the foil thickness and bump pitch from a given frequency response of the rotor. Also a scaled model of shaft, disc and bearing system is fabricated for testing.

Keywords: Foil bearings; Finite Difference scheme; Newmark method; Radial Basis Neural Network.

Table of Contents

List of Tables

List of Figures

Nomenclature

C	Bearing clearance (m)
E	Young's Modulus Of bump Foil (N/m^2)
f_x, f_y	Bearing reaction force in X and Y direction (N)
$\bar{h}$	Dimensionless film thickness (h/C)
k	Shaft stiffness (N/m)
l	Bump half length (m)
m_d	Disc mass (kg)
N	Journal Speed (rev/min)
p_{atm}	Atmospheric pressure (N/m^2)
$\bar{p}$	Dimensionless pressure
R	Bearing radius (m)
s	Bump pitch (m)
t_b	Bump foil thickness (m)
x_b, y_b	Journal eccentricities in X and Y directions at bearing centre (m)
x_d, y_d	Journal eccentricities in X and Y directions at disc centre (m)
X_b, Y_b	Eccentricity ratios in X and Y directions at bearing centre ($x_b / C, y_b / C$)
X_d, Y_d	Eccentricity ratios in X and Y directions at disc centre ($x_d / C, y_d / C$)
u_{im}	Unbalance eccentricity (m)
$\bar{z}$	Dimensionless axial coordinate (z / C)
α	Dimensionless compliance of bump foil
δ	Dimensionless top foil deflection
Λ	Bearing number
θ	Angular coordinate (rad)
ν	Viscosity of air (Ns/m^2)

τ	Dimensionless time (ωt)
υ	Poisson's ratio
ω	Angular velocity (rad/s)

Chapter 1

Introduction

Foil bearings commonly known as air foil bearings or gas foil bearings are very much suitable for high speed applications. These bearings have been in use and constantly developing since the 1960's. These bearings are being used in nearly every commercial aircraft because of their several advantages.

1.1. Overview of foil bearing

Foil bearings are very much similar in working as the other oil lubricated journal bearing. As with other hydrodynamic bearings, the weight of the shaft is supported by the high pressure region generated between the shaft and the stationary bearing. The load that can be supported is primarily a function of the relative surface speed, the area of the converging region, the shape of the clearance space between the rotor and top foil, the support structure stiffness and the viscosity of the lubricant (generally air for foil bearings). The gas films are practically isothermal because the heat dissipation rate of the bearing material is greater than the heat generation rate of the gas films.

In rotor dynamics, foil bearings found several advantages over conventional supports. These include reliability, no lubrication requirement, high/low temperature operation ability etc. In their simple structure, foil bearings have top-foil, corrugated bumps and bearing housing and such layered structure facilitates the stiffness and damping to the system. Bumps deform under hydrodynamic pressure load leading to converging wedge film between the shaft and bearing surface. The working fluid in foil bearing applications is usually air. Lower viscosity of air provides superior performance at high temperatures relative to oil and other liquid lubricants. Main limitation of foil bearings is that foil material losses strength at high temperatures resulting in drop of stiffness. The contact between the top foil and supporting bumps occurs at localized small areas that prevent heat dissipation. The role of the top foil is to generate air film and hydrodynamic lift force when shaft rotates. Therefore, it is important that stiffness of the top foil is sufficiently high to endure the hydrodynamic pressure. However, the portions of the top foil surface that are not in contact with the bumps have practically limited bending stiffness and deflect more when exposed to hydrodynamic pressure. Most of the studies neglected this deflection of the top foil.

Gas bearings can be classified in to following types:

- Aerostatic bearing
- Aerodynamic bearing

Aerostatic bearings support its entire designed load at zero speed. This effect results from its principle disadvantage i.e. it requires an external source to create the air film. The gas or the air is supplied into the bearing clearance at certain gauge pressure. The difference in the pressure causes the gas to flow form the supply line through the bearing gap to the atmosphere from the periphery of the bearing. The pressure generated in the clearance zone defines the load carrying capacity of the bearing and is limited only by the supply line pressure and material strength. The aerostatic bearing does not suffer from friction induced wear and in addition it has no starting and stopping friction.

In case of aerodynamic bearings also known as self-acting bearings, the air film is created by relative motion between two mating surfaces separated by a small distance. As the speed increases from zero to maximum a velocity induced pressure gradient is generated across the clearance. This pressure gradient between the surfaces creates the load carrying effect. As the load carrying capacity is dependent upon the relative speed at which the surface moves hence its does not support any load at zero speed. Since the bearing does not support any load at zero speed hence there is wear at start and towards the end of the process.

Advantages of foil bearing are as follows:

- Higher reliability: Machines based on foil bearing have to work with fewer number of parts to support the rotating assembly and since no lubricant is required for foil bearing it makes these bearings even more reliable. The air film between the journal the foil protects the bearings from wear.
- No scheduled maintenance: As we know that there is no lubrication requirement in foil bearings, checking and replacing of lubricant is not required. Hence saving the time and cost.
- Soft failure: since there is very less tolerance and clearance in foil bearing designed assembly in case of failure it restrains the shaft from moving too much containing the damage to bearing and shaft surface only.
- Environmental durability: Foil bearings can handle severe environmental condition such as dust and sand ingestions.

- High speed operations: foil bearing lets the compressors and turbines work at high speeds without any limitations. In fact, as the speed increase the load carrying capacity of these bearings also increases.
- Low and high temperature capabilities: Since these bearings use air, it helps these bearing to work in high temperature and low temperature environment.

1.2. **Literature Survey**

Several works described the use of foil bearings in rotors and described their dynamic principles. Some literature review is given below:

Balducchi et al. [1] presented the experimental analysis of the unbalance response produced by two rigid rotors which are slightly different in terms of mass supported by air foil bearings. The experiments are carried out between 50000 rpm and 100000 rpm and the displacements of the foils are shown in the waterfall plots.

Larsen and Santos [2] contributed a new method to calculate the steady state nonlinear response validating it both theoretically and experimentally. This paper represented a rotor system consisting of rigid rotor supported on segmented AFB. The bearing equation is solved using a Bubnov Galerkin finite element method. The stiffness and damping coefficients are estimated using a structural model which is later validated with experiments.

Larsen et al. [3] have primarily focused on the dynamic and quasa-static response of the bump foil structure and also the local response at its sliding points. The corrugated bump foils are used to introduce damping. The investigation of the structure is done both theoretically and experimentally. In the experimental analysis, the corrugated bump foil is fitted between two parallel contact surfaces. Theoretical analysis is done by mathematically modelling the structure using finite element method (FEM). The above given approach is used to compare the theoretical and experimental results.

Bonello and Pham [4] presented a method for the solution of state equations. The emergence of oil free turbomachinery is said to be marked by the emergence of air foil bearings (AFB). But with the advantages comes its ability to introduce nonlinearities which is why a reliable means is required for the dynamic analysis. This paper discusses a method to find the solution of state equations by employing two method (I) Finite Difference (II) Galerkin reduction method, it does not use a grid reducing the computational time considerably. Both FD and GR are cross verified by time domain simulations.

Yang et al. [5] have shown their extensive research on rotor system based on oil film journal bearings. In this paper a new method for the nonlinear dynamic analysis of rotor system has been discussed. This new method is based on the partial derivative method which has been extended to second order approximate to predict the nonlinear dynamic stiffness and damping coefficients of finite long journal bearings.

Jalali et al. [6] studied the dynamic behavior of the rotor system since at high speeds the rotor becomes vulnerable to vibrations. Both theoretical and experimental results have been compared. A 3d finite element model, 1D beam element model and an experimental setup is used to analyze the rotor system. The agreement between the experimental and theoretical results shows the efficiency of the Finite Element model. Campbell diagram, unbalance response, critical speeds etc. are used to represent the dynamic behavior of the system.

Bhore and Darpe [7] investigated the nonlinear behavior of a flexible rotor system based on aero foil bearings. The unsteady Reynold's equation is solved using power law hybrid scheme and Gauss-Sidle method. The dynamic equation of motion of the rotor system and the bearing equation is coupled using time domain orbit simulation. The non-linear behavior represented by Poincare maps and journal orbit and FFT curves. Various bifurcation parameters are used such as speed, unbalance eccentricity etc. to plot the bifurcation diagram of the dynamic behavior of the rotor system.

Bishwas et al [8] showed the transient analysis of multi lobe bearing. Different parameters were calculated using a turbulence model. For this a 3 lobe bearing was used in which the lobes were placed at 120 degrees. Speed at which the shaft rotates was assumed to be 80000 rpm. At higher speeds the oil property seems to converge which gave a new oil which with higher work efficiency.

Yu et al. [9] described the coupling of the pressure distribution, film thickness and the deformation of the foil structure through a numerical model which uses the finite element simulation. Finite element is used to solve the pressure distribution and deformation of foil and various parameters such as bearing number, number of perturbation, eccentricity ratio etc. are used to study the effects of their change on the bearing performance.

Chen et al. [10] presented a simple model of aerodynamic thrust foil gas bearing is suggested. Various experiments have been conducted on this bearing in a multi-functional

thrust bearing test rig. From the results it can be deduced that it has good load bearing capacity and stability.

Kumar and Kim [11] presented a new and highly efficient design of hydrostatic bearings as compared to their previous designs. A new test rig has also been developed for measuring load carrying capacity of these bearings at high speeds. Here the design uses corrugated bump foils. High load carrying capacity ensures the efficient hydrostatic levitation feature at lower speeds.

Lee et al [12] emphasized on the friction force generated between the bump and the surfaces with which it is in contact with. To understand the effect of friction on the performance of bearing this has attempted to create a static model in which the structure of the foil is modelled using FE method and an algorithm is developed which can predict the contact nodes condition and the direction in which the friction force is acting.

Arora et al. [13] suggested an experimental setup in this paper consists of only one bearing instead of conventional two bearings due to the requirement of high torque during the start and the stopping process. The experimental results show that the damping and the stiffness properties of the radial bearing have been identified accurately by following the mentioned experimental procedure.

Lee et al. [14] proposed a technique to obtain the dynamic response of the rotor system. A number of analytical techniques have been developed for the dynamic performance analysis of foil bearings. The dynamic performance of the bearings depends upon the coupling between the frictional motion of foil structure and the thin air film. Considering the coulomb friction, the author here has presented a nonlinear transient analysis method for performing the dynamic analysis of the bearing.

Kim and Park [15] provides a design, construction and testing of hydrostatic foil bearing (HAFB). The top foil deformation and dynamics of bump is modelled using a simple model and to predict the unbalance response time domain orbit simulation is used. The results are very much in agreement with the experimental results. This paper shows a HAFB which has higher load carrying capacity and apparently less wear during start and stops due to less torque than the hydrodynamic foil bearing.

Iordanoff et al. [16] focusses on studying the effect of this dry friction on the dynamic response of the bearing. The rotor equation is coupled with the Reynold's equation and the foil deformation equation. For different values of friction coefficient, the dynamic

response is studied. Critical speeds can be seen for high and low values of friction coefficient which seems to disappear for the medium values.

Andres and Kim [17] modelled the FB force as a 3rd order structural element. A symmetrically loaded rigid rotor system based on FB was tested in this paper and results were compared. It can be seen from the results that it produces multiple frequency responses within a certain range of speeds.

Lee et al. [18] suggested a new type of foil bearing which was named Viscoelastic Foil Bearing (VEFB). Both the conventional foil bearing and VEFB have been examined for structural dynamics and bending critical speeds. The test results show that viscous damping in VEFB was considerably higher than the conventional foil bearings and the stiffness coefficient is comparably equal or larger than the conventional FB. The increase in damping due to viscoelastic foil helps in reducing the vibrations at the critical speed.

Howard and Dykas [19] gave the design for the journal of turbomachines. With increase in speed the temperature also increases which in turn results in the non-uniform expansion of the shaft which in turn ends in vinous heating of the gas film which leads to high speed rub which damages the journal and the bearing. Hence a design consideration is required for the journal.

Dellacorte and Valco [20] proposed a new method for load carrying estimation of the foil bearing called 'Rule of thumb'. ROT introduced a load carrying coefficient D which was derived empirically and it relates load carrying capacity with bearing speed and physical attributes. Load carrying capacity is a linear function of projected area of the bearing and bearing velocity.

1.3. **Objectives of the work**

This work is focused on the foil bearing and its effect on the response of the rotor system. The objectives of the work are as follows:

- Discretization of Reynold's equation
- Steady state analysis of foil bearing by ignoring the time dependent terms in Reynold's equation.
- Evaluating the foil bearing forces
- Finding the solution to the coupled equation of motion of the rotor system and transient foil bearing forces.
- Evaluating the dynamic response of foil bearing based rotor system.

- Preparing a solid model and analysing in ANSYS for modal analysis.
- Preparing a neural network model to predict the bearing parameters based on the dynamic response of the rotor system.
- Prepare a scaled rotor bearing system for experimental dynamic analysis.

1.4. **Outline of the thesis**

This thesis consists of four chapters including the present chapter:

- CHAPTER 2 describes the basic mathematical model used for the theoretical analysis. It separated into three sub domains: foil bearing forces, discretization of Reynold's equation and dynamics of rotor system.
- CHAPTER 3 highlights the main results obtained from analysis. It presents the steady state pressure distribution, film thickness distribution and foil bearing forces and different parameters affecting foil bearing forces. It also presents the modal analysis and dynamic analysis results of the rotor system. A neural network model has also been presented in this chapter.
- CHAPTER 4 gives the summary and the future scope of the project.

Chapter 2

Mathematical Modelling

This chapter deals with the dynamic equations of foil bearing and the rotor modelling.

2.1. **Foil bearing forces**

The foil bearing consists of top foil, corrugated bumps and bearing housing. The top foil has a single sheet welded to the bearing sleeve from the trailing edge and the leading edge is free. The section of the bumps is modeled as plain geometry. Fig 2.1 shows the foil bearing components.

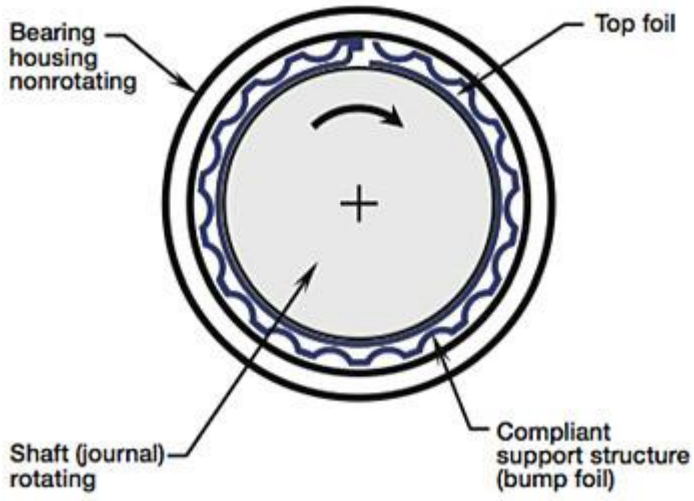

Figure 2-1 Foil bearing

Following are the assumptions considered:

- Change in film thickness in Z direction is negligible.
- Newtonian fluid
- No slip at the liquid solid boundary
- Constant coefficient of viscosity
- Isothermal condition
- Ideal but compressible gas flow.

Reynold's equation describing the generation of the gas pressure p within the film thickness h and for isothermal ideal gas, compressible fluids can be written as:

$$\frac{\partial}{\partial x}\left(\frac{\rho h^3}{12\nu}\frac{\partial p}{\partial x}\right)+\frac{\partial}{\partial z}\left(\frac{\rho h^3}{12\nu}\frac{\partial p}{\partial z}\right)=\frac{1}{2}\frac{\partial}{\partial x}(\rho(u_2-u_1)h)+\frac{\partial}{\partial t}(\rho h)+\frac{1}{2}\frac{\partial}{\partial z}(w_2-w_1) \quad (2.1)$$

$u_1, w_1 and\ u_2, w_2$ are velocities of outer and inner race

Since outer sleeve is immobile u_1=0 and u_2=u, also $w_1 = w_2 = 0$

In case of foil bearing the governing directions are z and θ. Hence converting the above Reynold's equation in polar coordinates

Substituting in eqn. (2.1)

$$x = R\theta, \quad \partial x = R\partial\theta, \ u = R\omega \quad (2.2)$$

$$\frac{\partial}{R\partial\theta}\left(\frac{\rho h^3}{12\nu}\frac{\partial p}{R\partial\theta}\right)+\frac{\partial}{\partial z}\left(\frac{\rho h^3}{12\nu}\frac{\partial p}{\partial z}\right)=\frac{R\omega}{2}\frac{\partial}{R\partial\theta}(\rho h)+\frac{\partial}{\partial t}(\rho h) \quad (2.3)$$

Reynold's equation in polar coordinates can be written as:

$$\frac{1}{R}\frac{\partial}{\partial\theta}\left(\frac{\rho h^3}{12\nu}\frac{\partial p}{R\partial\theta}\right)+\frac{\partial}{\partial z}\left(\frac{\rho h^3}{12\nu}\frac{\partial p}{\partial z}\right)=\frac{\omega}{2}\frac{\partial}{\partial\theta}(\rho h)+\frac{\partial}{\partial t}(\rho h) \quad (2.4)$$

According to ideal gas equation,

$$\rho = \frac{p}{R_{gas}T} \quad (2.5)$$

Substituting the value of ρ in equation (2.4) we get,

$$\frac{1}{R}\frac{\partial}{\partial\theta}\left(\frac{ph^3}{12\nu R_{gas}T}*\frac{1}{R}\frac{\partial p}{\partial\theta}\right)+\frac{\partial}{\partial z}\left(\frac{ph^3}{12\nu R_{gas}T}*\frac{\partial p}{\partial z}\right)=\frac{\omega}{2}\frac{\partial}{\partial\theta}\left(\frac{ph}{R_{gas}T}\right)+\frac{\partial}{\partial t}\left(\frac{ph}{R_{gas}T}\right) \quad (2.6)$$

Multiplying both sides by $R^2 R_{gas}$

$$\frac{\partial}{\partial\theta}\left(\frac{ph^3}{12\nu T}\frac{\partial p}{\partial\theta}\right)+R^2\frac{\partial}{\partial z}\left(\frac{ph^3}{12\nu T}\frac{\partial p}{\partial z}\right)=\frac{\omega R^2}{2}\frac{\partial}{\partial\theta}\left(\frac{ph}{T}\right)+R^2\frac{\partial}{\partial t}\left(\frac{ph}{T}\right) \quad (2.7)$$

Converting the polar form into non-dimensional form with following parameters:

Non-dimensional pressure $\bar{p} = \frac{p}{p_{atm}}$

Non dimensional film thickness $\bar{h} = \frac{h}{C}$

Similarly, $\bar{z} = \frac{z}{\frac{L}{2}}$, $\bar{v} = \frac{v}{v_0}$, $\bar{T} = \frac{T}{T_0}$

Substituting these values in the equation (2.7)

$$\frac{1}{R^2}\frac{\partial}{\partial\theta}\left(\frac{\bar{p}p_{atm}(\bar{h}C)^3}{12\bar{v}v_0\bar{T}T_0}\frac{\partial}{\partial\theta}(\bar{p}p_{atm})\right)+\frac{2\partial}{\partial(\bar{z}L)}\left(\frac{\bar{p}p_{atm}(\bar{h}C)^3}{12\bar{v}v_0\bar{T}T_0}\frac{2\partial}{\partial(\bar{z}L)}(\bar{p}p_{atm})\right)= \frac{w}{2}\frac{\partial}{\partial\theta}\left(\frac{\bar{p}p_{atm}\bar{h}C}{\bar{T}T_0}\right)+\frac{\partial}{\partial\tau}\left(\frac{\bar{p}p_{atm}\bar{h}C}{\bar{T}T_0}\right) \quad (2.8)$$

Multiplying both sides by R^2 we get,

$$\frac{\partial}{\partial\theta}\left(\frac{\bar{p}p_{atm}(\bar{h}C)^3}{12\bar{v}v_0\bar{T}T_0}\frac{\partial}{\partial\theta}(\bar{p}p_{atm})\right)+\left(\frac{2R}{L}\right)^2\frac{\partial}{\partial(\bar{z})}\left(\frac{\bar{p}p_{atm}(\bar{h}C)^3}{12\bar{v}v_0\bar{T}T_0}\frac{\partial}{\partial(\bar{z})}(\bar{p}p_{atm})\right)= \frac{wR^2}{2}\frac{\partial}{\partial\theta}\left(\frac{\bar{p}p_{atm}\bar{h}C}{\bar{T}T_0}\right)+R^2\frac{\partial}{\partial\tau}\left(\frac{\bar{p}p_{atm}\bar{h}C}{\bar{T}T_0}\right) \quad (2.9)$$

Assuming isothermal and iso-viscous condition i.e. $\bar{v}=1, \bar{T}=1$ we get,

$$\frac{\partial}{\partial\theta}\left(\frac{\bar{p}p_{atm}(\bar{h}C)^3}{12v_0T_0}\frac{\partial}{\partial\theta}(\bar{p}p_{atm})\right)+\left(\frac{2R}{L}\right)^2\frac{\partial}{\partial(\bar{z})}\left(\frac{\bar{p}p_{atm}(\bar{h}C)^3}{12v_0T_0}\frac{\partial}{\partial(\bar{z})}(\bar{p}p_{atm})\right)= \frac{wR^2}{2}\frac{\partial}{\partial\theta}\left(\frac{\bar{p}p_{atm}\bar{h}C}{T_0}\right)+R^2\frac{\partial}{\partial\tau}\left(\frac{\bar{p}p_{atm}\bar{h}C}{T_0}\right) \quad (2.10)$$

Simplifying

$$\frac{p_{atm}C^3}{12v_0T_0}\frac{\partial}{\partial\theta}(\bar{p}\bar{h}^3\frac{\partial}{\partial\theta}(\bar{p}p_{atm}))+\frac{p_{atm}C^3}{12v_0T_0}\left(\frac{2R}{L}\right)^2\frac{\partial}{\partial(\bar{z})}(\bar{p}\bar{h}^3\frac{\partial}{\partial(\bar{z})}(\bar{p}))= \frac{wR^2p_{atm}C}{2T_0}\frac{\partial}{\partial\theta}(\bar{p}\bar{h})+\frac{R^2p_{atm}C}{T_0}\frac{\partial}{\partial\tau}(\bar{p}\bar{h}) \quad (2.11)$$

Multiplying both sides by $\frac{p_{atm}C^3}{12v_0T_0}$

Reynold's equation for compressible fluids with isothermal condition may be written as:

$$\frac{\partial}{\partial\theta}(\bar{p}\bar{h}^3\frac{\partial\bar{p}}{\partial\theta})+\frac{\partial}{\partial\bar{z}}(\bar{p}\bar{h}^3\frac{\partial\bar{p}}{\partial\bar{z}})=\Lambda\frac{\partial}{\partial\theta}(\bar{p}\bar{h})+2\Lambda\frac{\partial}{\partial\tau}(\bar{p}\bar{h}) \quad (2.12)$$

Where Λ is compressibility number or bearing number which is given as

$$\Lambda=\frac{6wv_0}{p_{atm}}\left(\frac{R}{C}\right)^2 \quad (2.12a)$$

In case of foil bearing, the bump foils upon pressurizing gets deflected by δ and create more space. Hence the film thickness for foil bearing can be written as:

$$\bar{h} = 1 - X_b cos\theta - Y_b sin\theta + \delta \quad (2.13)$$

Where X_b ,Y_b are eccentricity ratios in X and Y directions

δ= bump foil deflection which is a function of pressure and dimensionless compliance of the bump foil bearing

For steady state,

$$\delta = \alpha\,(\bar{p}\,(\theta,z)-1 \quad (2.14)$$

α is compliance number which can be written as

$$\alpha = \frac{2*p_{atm}*s}{C*E} * (\frac{l}{t})^3 * (1-\vartheta^2) \quad (2.15)$$

For unsteady state the deflection of the foil is a function of time.

$$\delta^{\tau} = \frac{C_{bump}}{C_{bump} + K_{bump}\Delta\tau}\delta^{\tau-\Delta\tau} + \frac{\Delta\tau}{C_{bump} + K_{bump}\Delta\tau}\overline{p^{\tau}} \quad (2.16)$$

Where C_{bump} and K_{bump} are damping and stiffness coefficient of the bump foil

$$K_{bump} = \frac{1}{\alpha}, C_{bump} = \frac{\eta}{\upsilon}K_{bump}$$

η =loss factor, υ =frequency ratio

The Reynold's equation is solved with the following boundary condition:

$$\bar{p}\left(z = \pm\frac{L}{2R}, \theta\right) = 1$$
$$\bar{p}(z, \theta = \pi) = 1$$
$$\overline{p} = (z, \theta = 0) = \bar{p}(z, \theta = 2\pi) = 1 \quad (2.17)$$

The resulting pressure is obtained by using finite difference method and the load carrying capacity of the bearing is obtained in x and y directions as follows:

$$f_x = \int_0^{2\pi}\int_0^{L/R} p\cos\theta d\theta d\bar{z}$$
$$f_y = \int_0^{2\pi}\int_0^{L/R} p\sin\theta d\theta d\bar{z} \quad (2.18)$$

To obtain the bearing forces we require the pressure distribution in the bearing which can be obtained by solving the Reynold's equation.

2.2. **Discretization of Reynold's equation**

Here the Reynold's equation is solved by discretization using finite difference method. Finite difference scheme is of three types:

- Forward difference
- Central difference
- Backward difference

Central difference scheme has been utilized here to evaluate the pressure distribution in the bearings.

The grid over which the Reynold's equation is discretized is shown below:

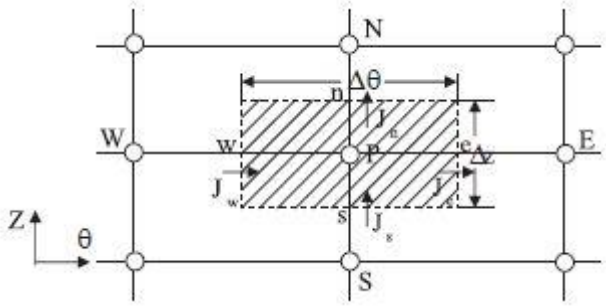

Figure 2-2 Discretization grid

According to central difference scheme:

$$\begin{aligned}
\frac{\partial \bar{p}}{\partial \theta} &= \frac{\bar{p}(i+1, j)-\bar{p}(i-1, j)}{2\Delta\theta} \\
\frac{\partial^2 \bar{p}}{\partial \theta^2} &= \frac{\bar{p}(i+1, j)-2\bar{p}(i, j)+\bar{p}(i-1, j)}{(\Delta\theta)^2} \\
\frac{\partial \bar{p}}{\partial \bar{z}} &= \frac{\bar{p}(i, j+1)-\bar{p}(i, j-1)}{2\Delta\bar{z}} \\
\frac{\partial^2 \bar{p}}{\partial \bar{z}^2} &= \frac{\bar{p}(i, j+1)-2\bar{p}(i, j)+\bar{p}(i, j-1)}{(\Delta\bar{z})^2}
\end{aligned} \tag{2.19}$$

2.2.1. Steady state Reynold's equation discretization

Reynold's equation for steady state

$$\frac{\partial}{\partial \theta}(\bar{p}\bar{h}^3\frac{\partial \bar{p}}{\partial \theta})+\frac{\partial}{\partial \bar{z}}(\bar{p}\bar{h}^3\frac{\partial \bar{p}}{\partial \bar{z}})=\Lambda\frac{\partial}{\partial \theta}(\bar{p}\bar{h}) \tag{2.20}$$

Discretizing the equation (2.7) using central difference scheme

A+B=C

Where

$$A=\frac{\partial}{\partial\theta}\left(\bar{p}\bar{h}^3\frac{\partial\bar{p}}{\partial\theta}\right) \qquad C=\Lambda\frac{\partial}{\partial\theta}(\bar{p}\bar{h})$$

$$B=\frac{\partial}{\partial\bar{z}}(\bar{p}\bar{h}^3\frac{\partial\bar{p}}{\partial\bar{z}})$$

$$A=\bar{p}\bar{h}^3\frac{\partial^2\bar{p}}{\partial\theta^2}+\bar{h}^3\frac{\partial\bar{p}}{\partial\theta}*\frac{\partial\bar{p}}{\partial\theta}+3\bar{p}\bar{h}^2\frac{\partial\bar{h}}{\partial\theta}*\frac{\partial\bar{p}}{\partial\theta} \tag{2.21}$$

$$B=\bar{p}\bar{h}^3\frac{\partial^2\bar{p}}{\partial\bar{z}^2}+\bar{h}^3\frac{\partial\bar{p}}{\partial\bar{z}}*\frac{\partial\bar{p}}{\partial\bar{z}} \tag{2.22}$$

$$C=\Lambda(\bar{p}\frac{\partial\bar{h}}{\partial\theta}+\bar{h}\frac{\partial\bar{p}}{\partial\theta}) \tag{2.23}$$

Let j represent z direction and i represent θ direction

Applying central difference scheme to A

$$A=\begin{aligned}&\bar{p}(i,j)*\bar{h}^3(i,j)*(\frac{\bar{p}(i+1,j)-2*\bar{p}(i,j)+\bar{p}(i-1,j)}{(\Delta\theta)^2})+\bar{h}^3(i,j)*(\frac{\bar{p}(i+1,j)-\bar{p}(i-1,j)}{2*\Delta\theta})^2\\&+3*\bar{p}(i,j)*\bar{h}^2(i,j)*(\frac{\bar{h}(i+1,j)-\bar{h}(i-1,j)}{2*\Delta\theta})*(\frac{\bar{p}(i+1,j)-\bar{p}(i-1,j)}{2*\Delta\theta})\end{aligned} \tag{2.24}$$

Applying central difference scheme to B

$$B=\bar{p}(i,j)*\bar{h}^3(i,j)*(\frac{\bar{p}(i,j+1)-2*\bar{p}(i,j)+\bar{p}(i,j-1)}{(\Delta\bar{z})^2})+\bar{h}^3(i,j)*(\frac{\bar{p}(i,j+1)-\bar{p}(i,j-1)}{2*\Delta\bar{z}})^2 \tag{2.25}$$

Applying central difference scheme to C

$$C=\Lambda*(\bar{p}(i.j)*(\frac{\bar{h}(i+1,j)-\bar{h}(i-1,j)}{2\Delta\theta})+\bar{h}(i,j)*(\frac{\bar{p}(i+1,j)-\bar{p}(i-1,j)}{2\Delta\theta})) \tag{2.26}$$

A+B-C=0

By rearranging the terms, we get,

$$\frac{\partial^2 \bar{p}}{\partial \theta^2}+\frac{\partial^2 \bar{p}}{\partial \bar{z}^2}=-\frac{3}{\bar{h}}\left(\frac{\partial \bar{p}}{\partial \theta}*\frac{\partial \bar{h}}{\partial \theta}\right)-\frac{1}{\bar{p}}\left(\left(\frac{\partial \bar{p}}{\partial \theta^2}\right)+\left(\frac{\partial \bar{p}}{\partial \bar{z}^2}\right)\right)+\frac{\Lambda}{\bar{h}^3}*\frac{\partial \bar{h}}{\partial \theta}+\frac{\Lambda}{\bar{p}\bar{h}^2}\frac{\partial \bar{p}}{\partial \theta} \tag{2.27}$$

$$\text{LHS}=\left(\frac{\bar{p}(i+1,j)-2\bar{p}(i,j)+\bar{p}(i-1,j)}{\Delta\theta^2}\right)+\left(\frac{\bar{p}(i,j+1)-2\bar{p}(i,j)+\bar{p}(i,j-1)}{\Delta\bar{z}^2}\right) \tag{2.28}$$

$$\begin{aligned}\text{RHS}=&-\frac{1}{\bar{p}(i,j)}\left[\left(\frac{\bar{p}(i+1,j)-\bar{p}(i-1,j)}{2\Delta\theta}\right)^2+\left(\frac{\bar{p}(i,j+1)-\bar{p}(i,j-1)}{2\Delta\bar{z}}\right)^2\right]\\&-\frac{3}{\bar{h}(i,j)}\left[\frac{\bar{h}(i+1,j)-\bar{h}(i-1,j)}{2\Delta\theta}*\frac{\bar{p}(i+1,j)-\bar{p}(i-1,j)}{2\Delta\theta}\right]\\&+\frac{\Lambda}{\bar{h}^3(i,j)}*\frac{\bar{h}(i+1,j)-\bar{h}(i-1,j)}{2\Delta\theta}+\frac{\Lambda}{\bar{p}(i,j)\bar{h}^2(i,j)}\frac{\bar{p}(i+1,j)-\bar{p}(i-1,j)}{2\Delta\theta}\end{aligned} \tag{2.29}$$

Rearranging the equation in terms of $\bar{p}(i,j)$

$$\bar{p}^2(i,j)\left(\frac{2}{\Delta\theta^2}+\frac{2}{\Delta\bar{z}^2}\right)+\bar{p}(i,j)\left[\begin{array}{l}-\dfrac{\bar{p}(i+1,j)-\bar{p}(i-1,j)}{\Delta\theta^2}-\dfrac{\bar{p}(i,j+1)-\bar{p}(i,j-1)}{\Delta\bar{z}^2}\\-\dfrac{3}{\bar{h}(i,j)}*\dfrac{\bar{h}(i+1,j)-\bar{h}(i-1,j)}{2\Delta\theta}*\dfrac{\bar{p}(i+1,j)-\bar{p}(i-1,j)}{2\Delta\theta}\\+\dfrac{\Lambda}{\bar{h}^3(i,j)}*\dfrac{\bar{h}(i+1,j)-\bar{h}(i-1,j)}{2\Delta\theta}\end{array}\right]$$

$$-\left[\left(\frac{\bar{p}(i+1,j)-\bar{p}(i-1,j)}{2\Delta\theta}\right)^2+\left(\frac{\bar{p}(i,j+1)-\bar{p}(i,j-1)}{2\Delta\bar{z}}\right)^2\right]+\frac{\Lambda}{\bar{h}^2(i,j)}*\frac{\bar{p}(i+1,j)-\bar{p}(i-1,j)}{2\Delta\theta}=0 \tag{2.30}$$

Equation (2.31) can be rewritten as a quadratic equation

$$P*\bar{p}^2(i,j)+Q*\bar{p}(i,j)+R=0 \tag{2.31}$$

This equation is solved and checked for convergence to get the pressure distribution.

2.2.2. Transient Reynold's equation discretization

Applying the central difference scheme to Reynold's Equation

Reynold's equation for compressible fluid

$$\frac{\partial}{\partial\theta}\left(\bar{p}\bar{h}^3\frac{\partial \bar{p}}{\partial\theta}\right)+\frac{\partial}{\partial\bar{z}}\left(\bar{p}\bar{h}^3\frac{\partial \bar{p}}{\partial\bar{z}}\right)=\Lambda\frac{\partial}{\partial\theta}(\bar{p}\bar{h})+2\Lambda\frac{\partial}{\partial\tau}(\bar{p}\bar{h}) \tag{2.32}$$

Let's denote the above equation as

A+B=C+D

Where

$$A=\frac{\partial}{\partial\theta}\left(\bar{p}\bar{h}^3\frac{\partial\bar{p}}{\partial\theta}\right) \qquad C=\Lambda\frac{\partial}{\partial\theta}(\bar{p}\bar{h})$$

$$B=\frac{\partial}{\partial\bar{z}}(\bar{p}\bar{h}^3\frac{\partial\bar{p}}{\partial\bar{z}}) \qquad D=2\Lambda\upsilon\frac{\partial}{\partial\tau}(\bar{p}\bar{h})$$

$$A=\bar{p}\bar{h}^3\frac{\partial^2\bar{p}}{\partial\theta^2}+\bar{h}^3\frac{\partial\bar{p}}{\partial\theta}*\frac{\partial\bar{p}}{\partial\theta}+3\bar{p}\bar{h}^2\frac{\partial\bar{h}}{\partial\theta}*\frac{\partial\bar{p}}{\partial\theta}$$

Let j represent z direction and i represent θ direction

Applying central difference scheme to A

$$A=\begin{aligned}&\bar{p}(i,j)*\bar{h}^3(i,j)*\left(\frac{\bar{p}(i+1,j)-2*\bar{p}(i,j)+\bar{p}(i-1,j)}{(\Delta\theta)^2}\right)+\bar{h}^3(i,j)*\left(\frac{\bar{p}(i+1,j)-\bar{p}(i-1,j)}{2*\Delta\theta}\right)^2\\&+3*\bar{p}(i,j)*\bar{h}^2(i,j)*\left(\frac{\bar{h}(i+1,j)-\bar{h}(i-1,j)}{2*\Delta\theta}\right)*\left(\frac{\bar{p}(i+1,j)-\bar{p}(i-1,j)}{2*\Delta\theta}\right)\end{aligned}$$

(2.33)

Applying central difference scheme to B

$$B=\bar{p}(i,j)*\bar{h}^3(i,j)*\left(\frac{\bar{p}(i,j+1)-2*\bar{p}(i,j)+\bar{p}(i,j-1)}{(\Delta\bar{z})^2}\right)+\bar{h}^3(i,j)*\left(\frac{\bar{p}(i,j+1)-\bar{p}(i,j-1)}{2*\Delta\bar{z}}\right)^2$$

(2.34)

Applying central difference scheme to C

$$C=\Lambda*\left(\bar{p}(i.j)*\left(\frac{\bar{h}(i+1,j)-\bar{h}(i-1,j)}{2\Delta\theta}\right)+\bar{h}(i,j)*\left(\frac{\bar{p}(i+1,j)-\bar{p}(i-1,j)}{2\Delta\theta}\right)\right) \qquad (2.35)$$

Applying central difference scheme to D

$$D=2*\Lambda*\left(\frac{(p(i,j)*h(i,j))^{\tau}-(p(i,j)*h(i,j))^{\tau-\Delta\tau}}{\Delta\tau}\right) \qquad (2.36)$$

D=A+B-C

Putting the values of A, B, C and D

$$2*\Lambda*(\frac{(p(i,j)*h(i,j))^{\tau}-(p(i,j)*h(i,j))^{\tau-\Delta\tau}}{\Delta\tau})=$$

$$\bar{p}(i,j)*\bar{h}^3(i,j)*(\frac{\bar{p}(i+1,j)-2*\bar{p}(i,j)+\bar{p}(i-1,j)}{(\Delta\theta)^2})+\bar{h}^3(i,j)*(\frac{\bar{p}(i+1,j)-\bar{p}(i-1,j)}{2*\Delta\theta})^2$$

$$+3*\bar{p}(i,j)*\bar{h}^2(i,j)*(\frac{\bar{h}(i+1,j)-\bar{h}(i-1,j)}{2*\Delta\theta})*(\frac{\bar{p}(i+1,j)-\bar{p}(i-1,j)}{2*\Delta\theta})$$

$$\bar{p}(i,j)*\bar{h}^3(i,j)*(\frac{\bar{p}(i,j+1)-2*\bar{p}(i,j)+\bar{p}(i,j-1)}{(\Delta\bar{z})^2})+\bar{h}^3(i,j)*(\frac{\bar{p}(i,j+1)-\bar{p}(i,j-1)}{2*\Delta\bar{z}})^2$$

(2.37)

$$-\Lambda*(\bar{p}(i.j)*(\frac{\bar{h}(i+1,j)-\bar{h}(i-1,j)}{2\Delta\theta})+\bar{h}(i,j)*(\frac{\bar{p}(i+1,j)-\bar{p}(i-1,j)}{2\Delta\theta}))$$

$$2*\Lambda*(\frac{(\bar{p}(i,j)*\bar{h}(i,j))^{\tau}-(\bar{p}(i,j)*\bar{h}(i,j))^{\tau-\Delta\tau}}{\Delta\tau})=\text{A+B-C}$$

Rearranging the above equation in terms of $\bar{p}^{\tau}(i,j)$

$$(\bar{p}(i,j)*\bar{h}(i,j))^{\tau}-(\bar{p}(i,j)*\bar{h}(i,j))^{\tau-\Delta\tau}=\frac{\Delta\tau}{2\Lambda}(A+B-C) \quad (2.38)$$

$$(\bar{p}(i,j)*\bar{h}(i,j))^{\tau}=(\bar{p}(i,j)*\bar{h}(i,j))^{\tau-\Delta\tau}+\frac{\Delta\tau}{2\Lambda}(A+B-C) \quad (2.39)$$

$$\bar{p}^{\tau}(i,j)=\frac{1}{\bar{h}(i,j))^{\tau}}((\bar{p}(i,j)*\bar{h}(i,j))^{\tau-\Delta\tau}+\frac{\Delta\tau}{2\Lambda}(A+B-C)) \quad (2.40)$$

Now we have linear equation in form of pressure which we can solve using Gauss Sidle method.

Alternatively, we can discretize Reynold's equation using half note method.

$$\frac{\partial}{\partial\theta}(\bar{p}\bar{h}^3\frac{\partial\bar{p}}{\partial\theta})+\frac{\partial}{\partial\bar{z}}(\bar{p}\bar{h}^3\frac{\partial\bar{p}}{\partial\bar{z}})=\Lambda\frac{\partial}{\partial\theta}(\bar{p}\bar{h})+2\Lambda\frac{\partial}{\partial\tau}(\bar{p}\bar{h}) \quad (2.41)$$

Let's denote the above equation as

A+B=C+D

Where,

$$\text{A}=\frac{\partial}{\partial\theta}\left(\bar{p}\bar{h}^3\frac{\partial\bar{p}}{\partial\theta}\right)$$

A can be rewritten as,

$$A=\frac{\partial}{\partial\theta}\left(\bar{h}^3\frac{\partial\bar{p}^2}{\partial\theta}\right)$$

Expanding A in terms of i and j

A=

$$\frac{\bar{h}^3(i,\,j+0.5)*\bar{p}^2(i,\,j+1)-(\bar{h}^3(i,\,j+0.5)+\bar{h}^3(i,\,j-0.5))*\bar{p}^2(i,\,j)+\bar{h}^3(i,\,j-0.5)*\bar{p}^2(i,\,j-1)}{(\Delta\theta)^2}$$

(2.42)

$$B=\frac{\partial}{\partial\bar{z}}\left(\bar{h}^3\frac{\partial\bar{p}^2}{\partial\bar{z}}\right)$$

Expanding B in terms of i and j

B=

$$\frac{\bar{h}^3(i+0.5,\,j)*\bar{p}^2(i+1,\,j)-(\bar{h}^3(i+0.5,\,j)+\bar{h}^3(i-0.5,\,j))*\bar{p}^2(i,\,j)+\bar{h}^3(i-0.5,\,j)*\bar{p}^2(i-1,\,j)}{(\Delta\bar{z})^2}$$

(2.43)

$$C=\Lambda\frac{\partial}{\partial\theta}(\bar{p}\bar{h})$$

Expanding C in terms of i and j

$$C=\Lambda\left(\frac{\bar{p}(i,\,j+1)*\bar{h}(i,\,j+1)-\bar{p}(i,\,j-1)*\bar{h}(i,\,j-1)}{\Delta\theta}\right) \quad (2.44)$$

$$D=2\Lambda\frac{\partial}{\partial\tau}(\bar{p}\bar{h})$$

$$D=2\Lambda*\left(\frac{(\bar{p}(i,\,j)*\bar{h}(i,\,j))^{\tau}-(\bar{p}(i,\,j)*\bar{h}(i,\,j))^{\tau-\Delta\tau}}{\Delta\tau}\right) \quad (2.45)$$

A+B=C+D

$$\frac{\bar{h}^3(i,\,j+0.5)*\bar{p}^2(i,\,j+1)-(\bar{h}^3(i,\,j+0.5)+\bar{h}^3(i,\,j-0.5))*\bar{p}^2(i,\,j)+\bar{h}^3(i,\,j-0.5)*\bar{p}^2(i,\,j-1)}{(\Delta\theta)^2}$$

+

$$\frac{\bar{h}^3(i+0.5,j)*\bar{p}^2(i+1,j)-(\bar{h}^3(i+0.5,j)+\bar{h}^3(i-0.5,j))*\bar{p}^2(i,j)+\bar{h}^3(i-0.5,j)*\bar{p}^2(i-1,j)}{(\Delta\bar{z})^2}$$

$$= \Lambda(\frac{\bar{p}(i,j+1)*\bar{h}(i,j+1)-\bar{p}(i,j-1)*\bar{h}(i,j-1)}{\Delta\theta})+ \tag{2.46}$$

$$2\Lambda*(\frac{(\bar{p}(i,j)*\bar{h}(i,j))^{\tau}-(\bar{p}(i,j)*\bar{h}(i,j))^{\tau-\Delta\tau}}{\Delta\tau})$$

$$\text{A+B-C= } 2\Lambda*(\frac{(\bar{p}(i,j)*\bar{h}(i,j))^{\tau}-(\bar{p}(i,j)*\bar{h}(i,j))^{\tau-\Delta\tau}}{\Delta\tau})$$

$$\frac{\Delta\tau}{2\Lambda}(A+B-C)+(\bar{p}(i,j)*\bar{h}(i,j))^{\tau-\Delta\tau}=(\bar{p}(i,j)*\bar{h}(i,j))^{\tau} \tag{2.47}$$

$$(\bar{p}(i,j))^{\tau}=(\frac{\Delta\tau}{2\Lambda}(A+B-C)+(\bar{p}(i,j)*\bar{h}(i,j))^{\tau-\Delta\tau})*\frac{1}{(\bar{h}(i,j))^{\tau}} \tag{2.48}$$

Now we have a linear equation in terms of pressure. We can solve it using Gauss Seidle method

2.3. **Dynamics of rotor system**

The rotor bearing system shown in figure 2.2. It has a disc of mass m_d and the shaft has a half stiffness k. The disc unbalance is $u_{unbalance}$ and shaft speed is ω. The four dynamic equations are written from two half portions of the shaft as follows.

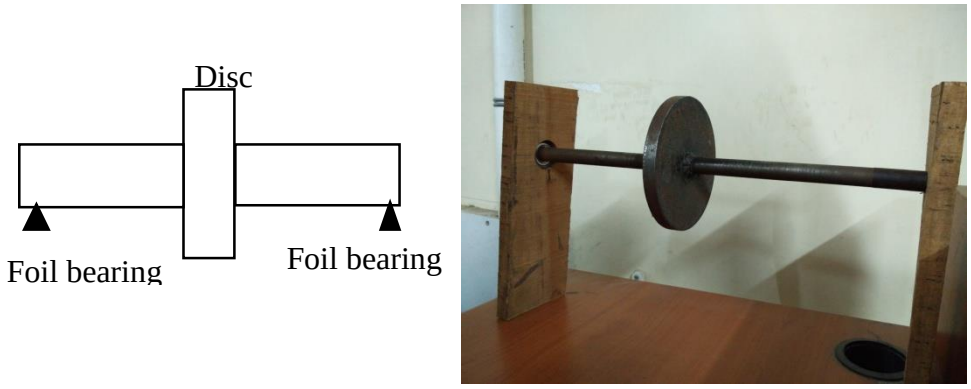

Figure 2-3 Single disc rotor model

The dynamics of the given rotor system is governed by following equations:

The dynamic equation of motion at disc node is given by:

$$m_{disc}\ddot{x}_d + k(x_d - x_b) = m_{disc} * u_{imbalance} * \omega^2 * \cos(\omega t) + m_{disc} * g \tag{2.49}$$

$$m_{disc}\ddot{y}_d + k(y_d - y_b) = m_{disc} * u_{imbalance} * \omega^2 * \sin(\omega t) \tag{2.50}$$

The dynamic equation at the bearing node is given by:

$$\begin{aligned} k(x_b - x_d) &= F_x \\ k(y_b - y_d) &= F_y \end{aligned} \tag{2.51}$$

Where k is shaft stiffness

x_d and y_d are eccentricity of the disc

x_b and y_b are eccentricity at the journal

For the simplicity of calculation and to remove the complexity, converting the above system of equations in non-dimensional form.

$$\ddot{X}_d = \frac{1}{m_d C\omega^2}(m_{disc} * u_{imbalance} * \omega^2 * \cos(\omega t) + m_{disc} * g - kC(X_d - X_b)) \tag{2.52}$$

$$\ddot{Y}_d = \frac{1}{m_d C\omega^2}(m_{disc} * u_{imbalance} * \omega^2 * \sin(\omega t) - kC(Y_d - Y_b)) \tag{2.53}$$

$$\begin{aligned} X_b &= \frac{1}{kC}(F_x + kCX_d) \\ Y_b &= \frac{1}{kC}(F_y + kCY_d) \end{aligned} \tag{2.54}$$

To solve the above system of equations we need to integrate them and for that purpose we are employing an algorithm known as Verlet algorithm.

With the initial values of X_b, Y_b, X_d and Y_d the new acceleration is calculated and after integrating equation 2.53 and 2.54 we get the following equations for velocity and displacement

$$\dot{X}_d(\tau+\Delta\tau) = \dot{X}_d(\tau) + \ddot{X}_d(\tau+\Delta\tau)*\Delta\tau$$
$$\dot{Y}_d(\tau+\Delta\tau) = \dot{Y}_d(\tau) + \ddot{Y}_d(\tau+\Delta\tau)*\Delta\tau$$
$$X_d(\tau+\Delta\tau) = X_d(\tau) + \dot{X}_d(\tau+\Delta\tau)*\Delta\tau + \frac{\Delta\tau^2}{2}\ddot{X}_d(\tau+\Delta\tau) \quad (2.55)$$
$$Y_d(\tau+\Delta\tau) = Y_d(\tau) + \dot{Y}_d(\tau+\Delta\tau)*\Delta\tau + \frac{\Delta\tau^2}{2}\ddot{Y}_d(\tau+\Delta\tau)$$

These values of X_d and Y_d and the bearing forces is then put in to equation 2.54 and 2.55 to get the new journal displacements.

$$X_b(\tau+\Delta\tau) = \frac{1}{kC}(F_x(\tau) + kCX_d(\tau+\Delta\tau) \quad (2.56)$$
$$Y_b(\tau+\Delta\tau) = \frac{1}{kC}(F_y(\tau) + kCY_d(\tau+\Delta\tau)$$

With these new values of X_b, Y_b we can calculate the new pressure distribution and the new bearing forces for the next time instant.

Alternatively, we can use Newmark's method to solve the differential equation of motion

Fig 2.3 shows the flowchart of the Newmark method with following constants

$$C0 = \frac{1}{\beta*\Delta t^2}$$
$$C1 = \frac{\chi}{\beta*\Delta t}$$
$$C2 = \frac{1}{\beta*\Delta t} \quad (2.57)$$
$$C3 = \frac{1}{2\beta} - 1$$
$$C4 = \frac{\chi}{\beta} - 1$$
$$C5 = \frac{\Delta t}{2}(\frac{\chi}{\beta} - 2)$$
$$C6 = \Delta t(1-\chi)$$
$$C7 = \chi*\Delta t$$

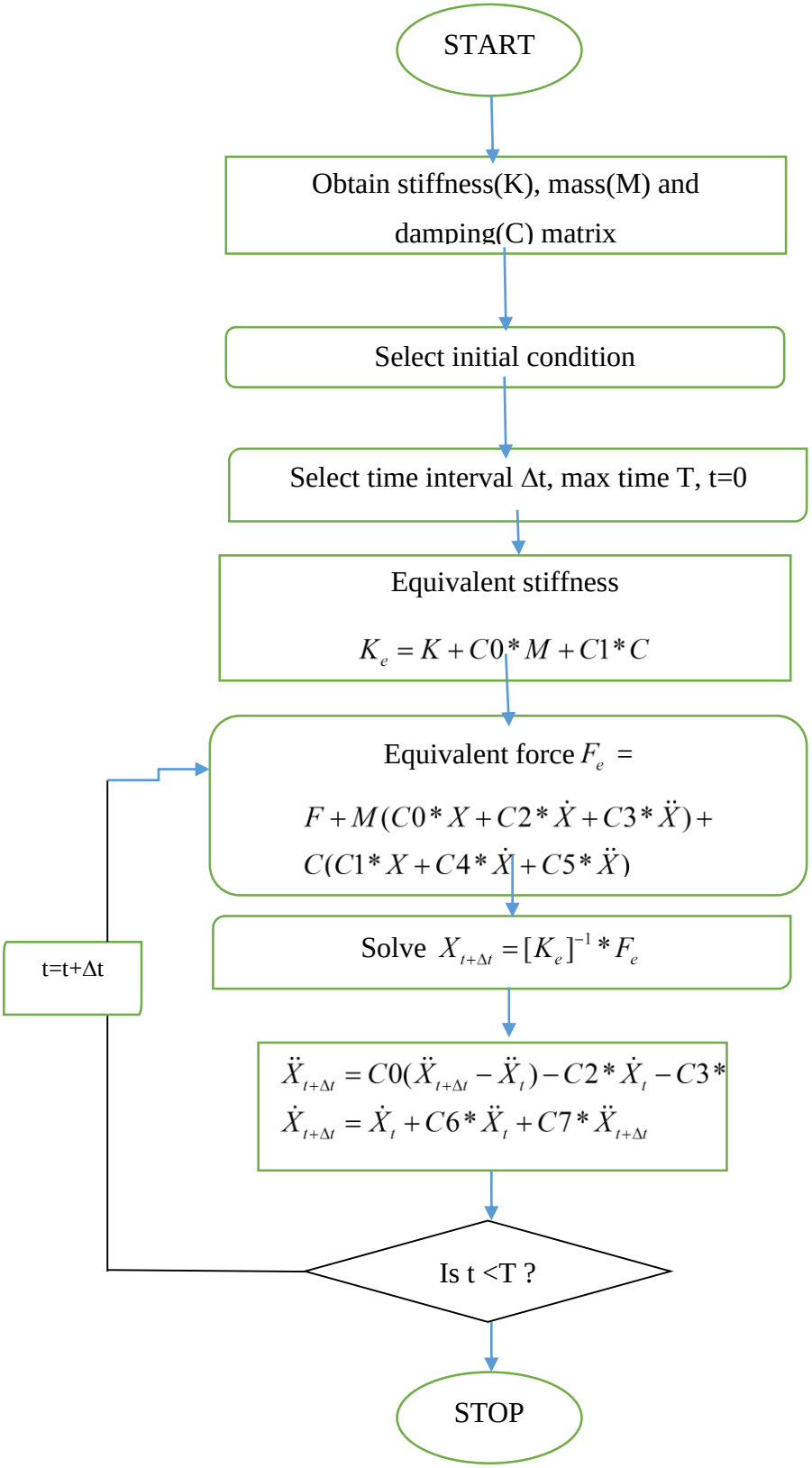

Figure 2-4 Newmark Method

Chapter 3

Results and Discussions

A foil bearing based rotor system is analyzed and its response is recorded. Effect of various parameters on these response is also analyzed. The input parameter which are used for the analysis can be seen in the table 3.1

Table 3-1 Input parameters considered [7]

S. No.	Input parameters	Value	Unit
1	Radial clearance	0.0318	mm
2	Bearing Radius	19.05	mm
3	Length of bearing	38.1	mm
4	Bump pitch	4.572	mm
5	Bump half length	1.778	mm
6	Bump foil thickness	0.108	mm
7	Poisson's ratio	0.29	-
8	Viscosity of lubricant	$1.78*10^{5}$	Pa-s
9	Modulus of elasticity of bump	21200	N/mm^2
10	Disc mass	3	kg

3.1. Steady state analysis of foil bearing

In this section, the results obtained from the developed Matlab program are presented.

3.1.1. Pressure distribution

Here the bearing is separately considered without rotor. Steady state analysis is done by discretizing the governing Reynold's equation using the finite difference scheme over a defined grid as shown in the mathematical modelling chapter. After the discretization pressure and film thickness is found out at every point of the bearing which gives us the pressure distribution in the bearing.

The pressure distribution in the bearing is shown in Fig 3.1:

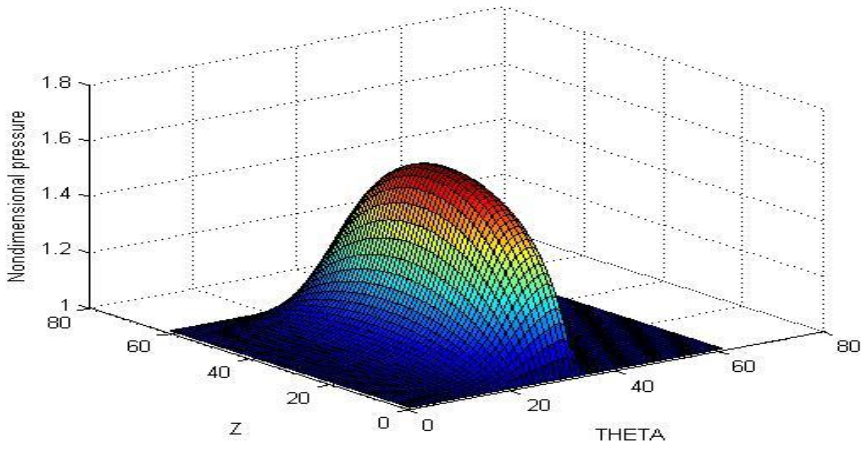

Figure 3-1 3-D pressure distribution

As it can be seen from both the figures that the pressure at the beginning and at the end is atmospheric. It rises gradually and then falls suddenly the moment it reaches its peak. The reason behind the atmospheric pressure at the beginning is that it is an aerodynamic bearing so it does not require any external pressure. As the theta value increases and the shaft starts to speed up and the pressure stars rising. After it reaches its peak the pressure generated is so high that top foil and bump foil comes in contact with each other which leads the pressure to drop significantly. Since the bump and the top foil are not joined together when the pressure drop leads to create a negative pressure zone they get separated from each other leading to the atmospheric pressure condition.

3.1.2. Film thickness distribution

The pressure distribution shown previously is dependent upon the film thickness distribution. Thinner the film gets the higher will be the pressure. Film thickness distribution in the bearing shows high thickness at the beginning since pressure at the beginning is atmospheric. As the pressure starts to rise it starts exerting more and more force which leads to reduction in the thickness of film. When the pressure is at its peak, the film thickness is at its lowest level. And at the end as can be seen from the figures that the pressure again becomes atmospheric which leads to thickening to the film. The film in this bearing is an air film which loses heat easily hence these bearings can be used in high temperature environment. Fig 3.2 shows the film thickness variation in a 3-D plot.

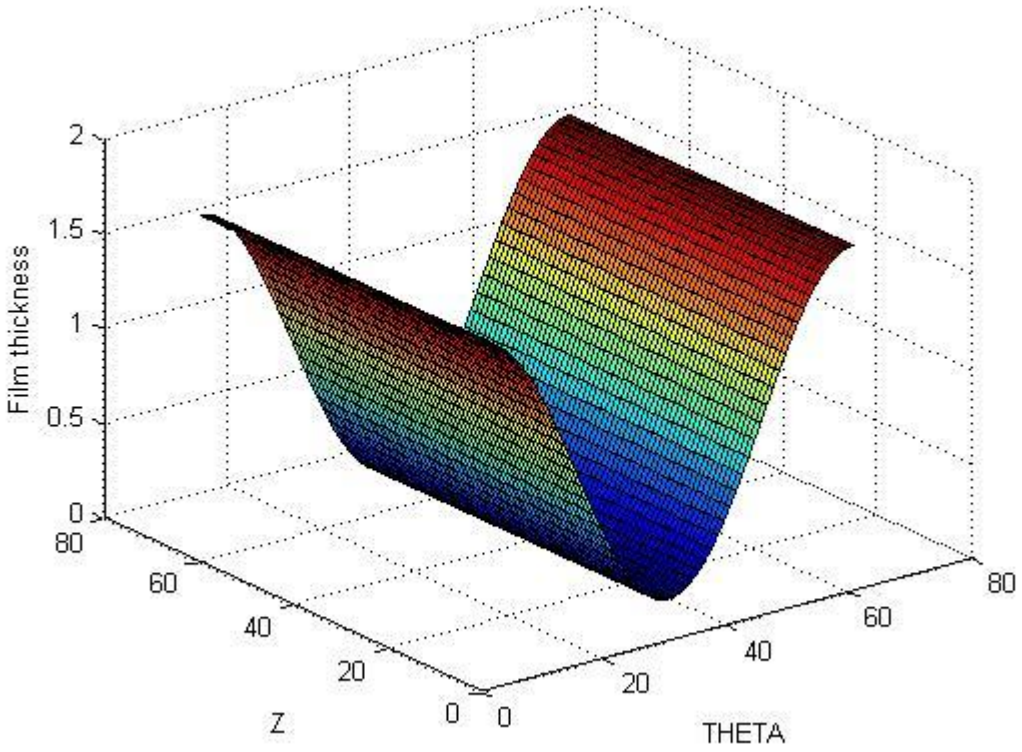

Figure 3-2 Film thickness distribution 3-D

3.1.3. Load carrying capacity

Fig 3.3 shows the variation of load carrying capacity as a function of eccentricity ratio.

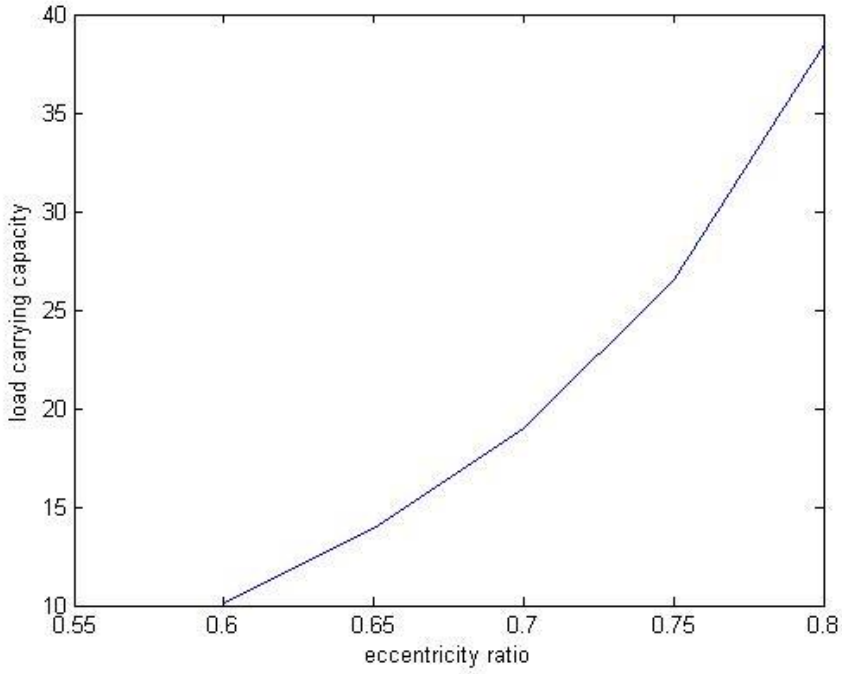

Figure 3-3 Load carrying capacity vs eccentricity ratio

It represents the variation of load carrying capacity of the foil bearing with respect to eccentricity ratio. As the eccentricity increases the film thickness increases which leads to the increase in pressure and with increase in pressure the load carrying capacity increases.

Fig 3.4 shows the variation of load carrying capacity with bearing number.

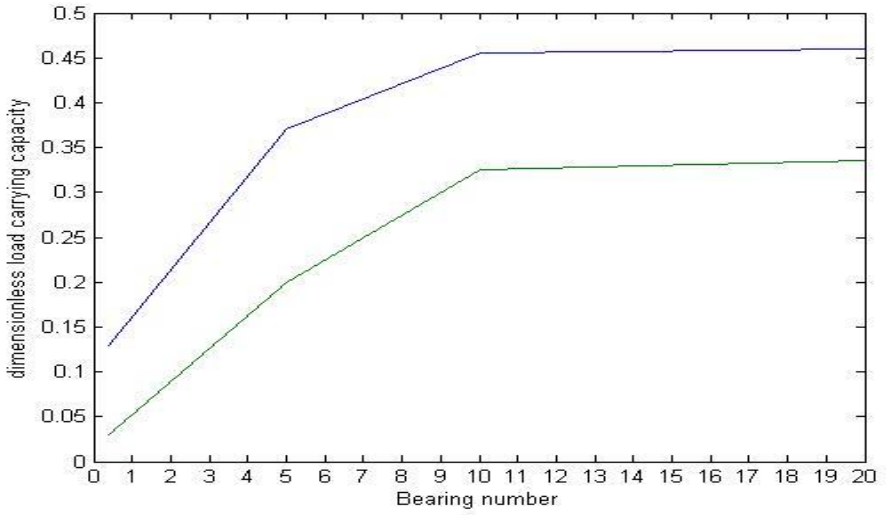

Figure 3-4 load carrying capacity vs bearing number

It shows the variation of load carrying capacity with respect to bearing number at different eccentricity ratio. At a constant eccentricity ratio, the load carrying capacity increases with the increase in bearing number for some values after that it becomes constant. The reason for this is that with increase in speed the bearing number increases and the component depending upon the bearing number which influence the pressure increases. These components can be seen in the mathematical modelling section. Now at high enough the pressure becomes very high and the value of the components influencing the pressure becomes very high. Now with increase in speed the bearing number increases but its effect becomes negligible due to high pressure.

3.2. **Modal analysis of rotor system**

Modal analysis of the rotor system is carried out to obtain the critical speeds of the rotor system and to obtain different mode shapes of the rotor system. With the knowledge of the critical speeds, we can design system accordingly so that it can withstand the vibration effects.

For the modal analysis, the rotor system has been prepared in the Solidworks as shown in Fig.3.5

(a) Top foil

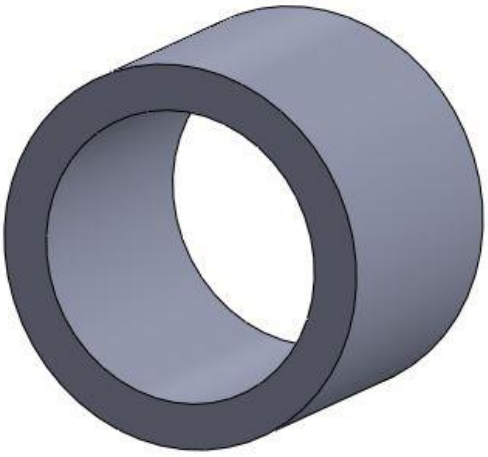

(b) Sleeve

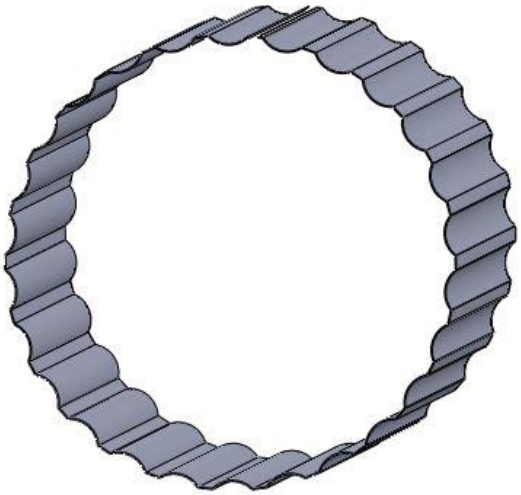

(c) Bump foil

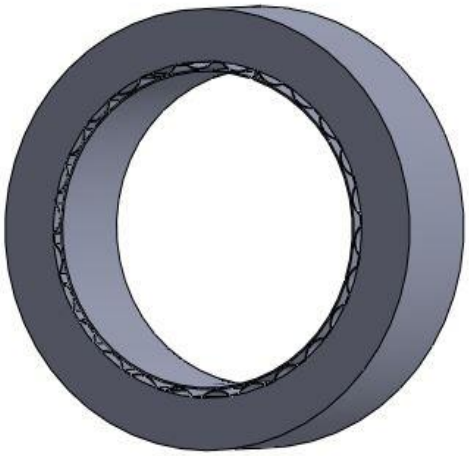

(d) Foil bearing assembly

Figure 3-5 Foil bearing model in Solidworks

Fig 3.6 shows the rotor with shaft and disc drawn in the Solidworks .

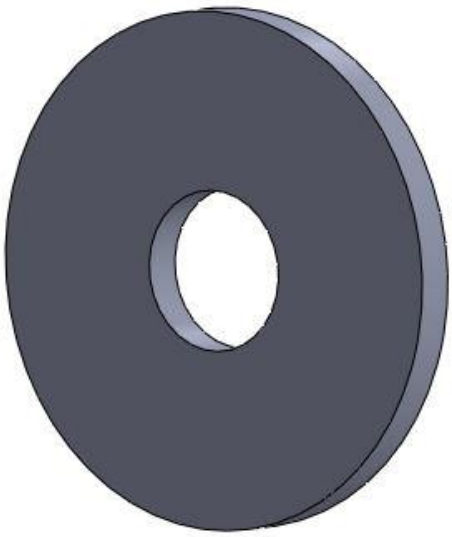

(a) Disc

(b) Shaft

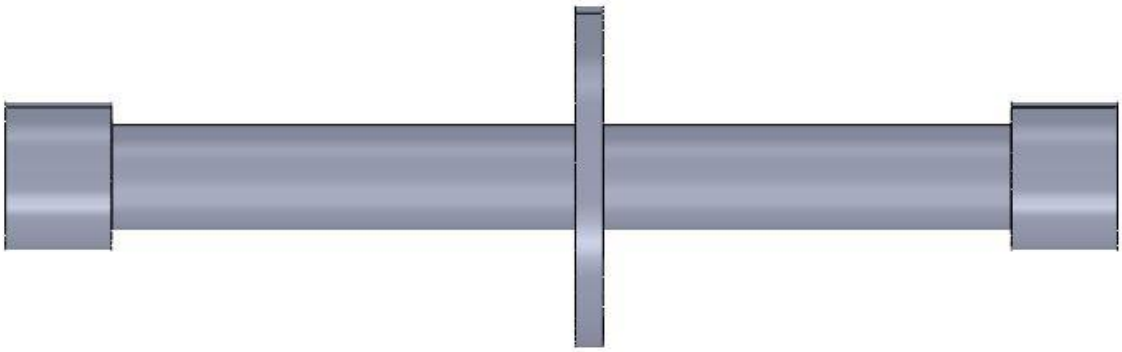

(c) Assembly of the entire parts

Figure 3-6 Foil bearing rotor system

The prepared model is imported in to ANSYS Workbench for the modal analysis and the natural frequencies obtained are reported in Table 3.2:

Table 3-2 critical speeds

S. No.	Critical speed(Hz)	Published data
1	322	318
2	418	405
3	4182	4165

Mode shape at one of these natural frequencies is shown in the figure 3.7

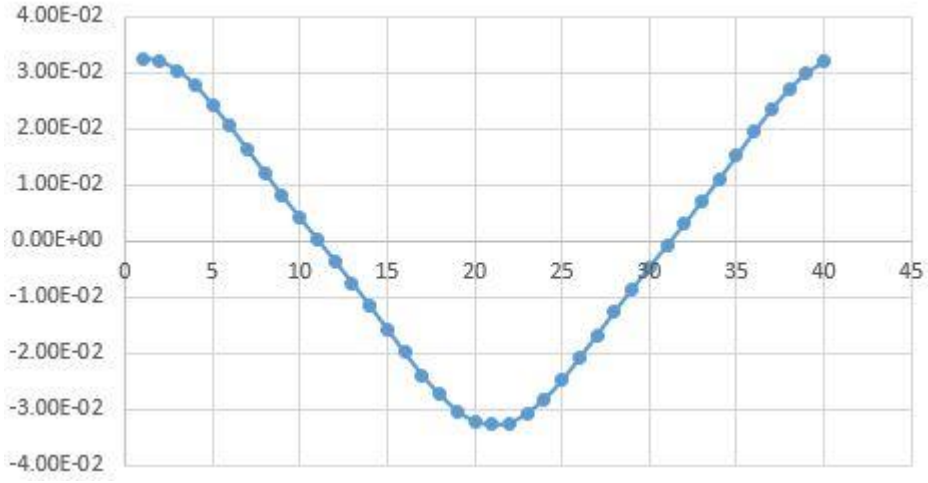

Figure 3-7 Mode Shape

3.3. **Dynamic analysis of rotor system**

Table 3.3 shows the specifications of rotor system considered in this work.

Table 3-3 Rotor System specification

S. no.	parameter	value
1	Length of shaft	400 mm
2	Diameter of shaft	38 mm
3	Modulus of Elasticity	200 GPa
4	Disc mass	3 kg

For the dynamic analysis the equation of motion of rotor system is coupled with the bearing force and the system of equation is solved by implicit integration technique. The implicit integration technique is used.

After solving the system of equations we get the displacement of journal in X and Y directions which are then plotted against each other to obtain the journal orbit.

Fast Fourier Transform (FFT) are used to obtain the frequency response curve.

Fig3.8 shows XY orbit plot of the rotor at bearing corresponding to shaft speed of 10000 rpm.

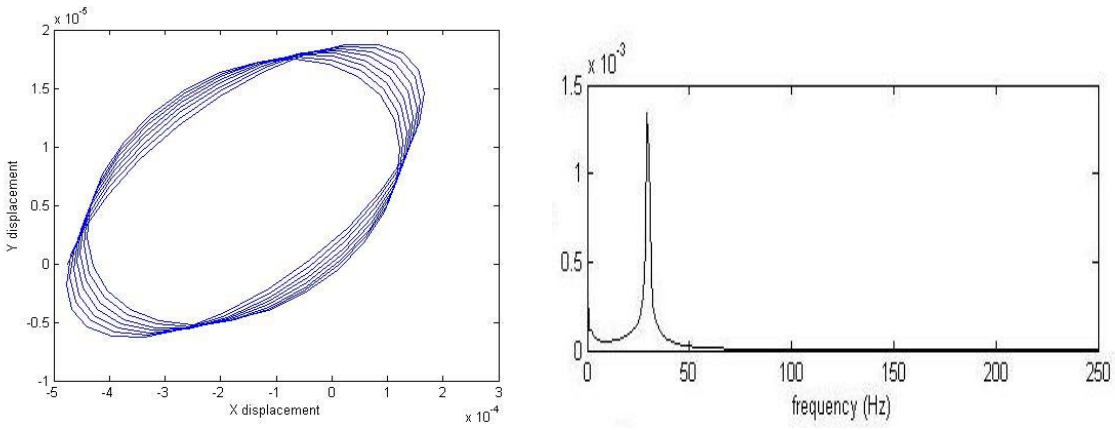

(a) Orbit plot (b) FFT curve in X direction

Figure 3-8 dynamic response at 10000 rpm

With $u_{imbalance} = 1*10^{-8} m$ above figure has been plotted. It seems that the system is harmonic fully and there is no instability. Similarly, Fig 3.9 shows the orbit plot and fft curve at 13000 rpm. It can be seen that as the speed increases the amplitude is decreasing moving towards more stable positon.

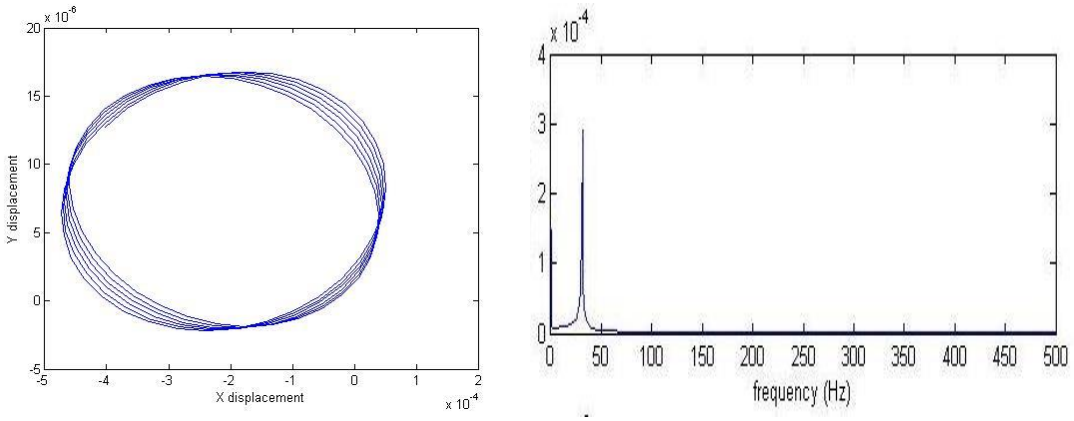

(a) orbit plot (b) FFT curve in X direction

Figure 3-9 dynamic response at 13000 rpm

Fig 3.10 shows the orbit plot and fft curve at 16000 rpm. As it can be seen from the figure that the system is stable and the amplitude of vibration is still decreasing making the system more stable. Similar effects can be seen in Fig. 3.11 which presents the orbit plot and FFT curve at 20000 rpm.

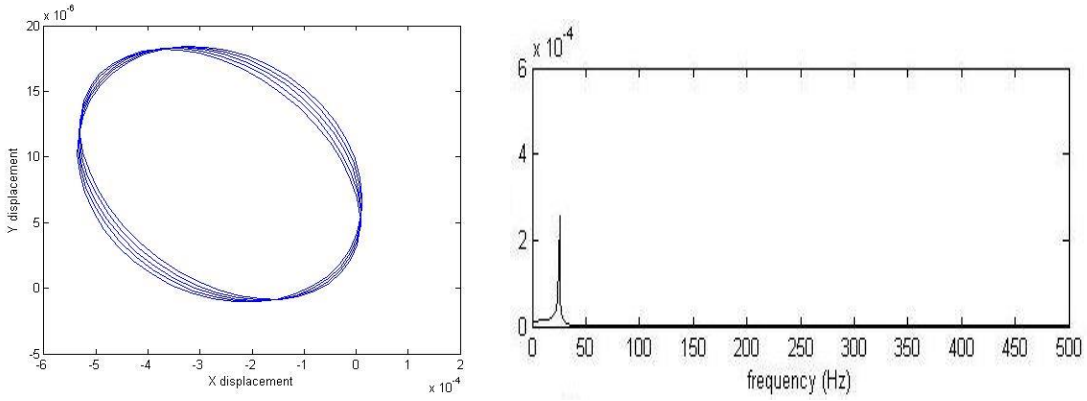

(a) Orbit plot (b) FFT curve in X direction

Figure 3-10 Dynamic response at 16000 rpm

At 16000 rpm the orbit of the disc is found to be changing directions as compared to at 10000 rpm fig 3.10 (a) and it can be seen from the FFT curve 3.10 (b) that the amplitude of vibration is still decreasing making the system more stable.

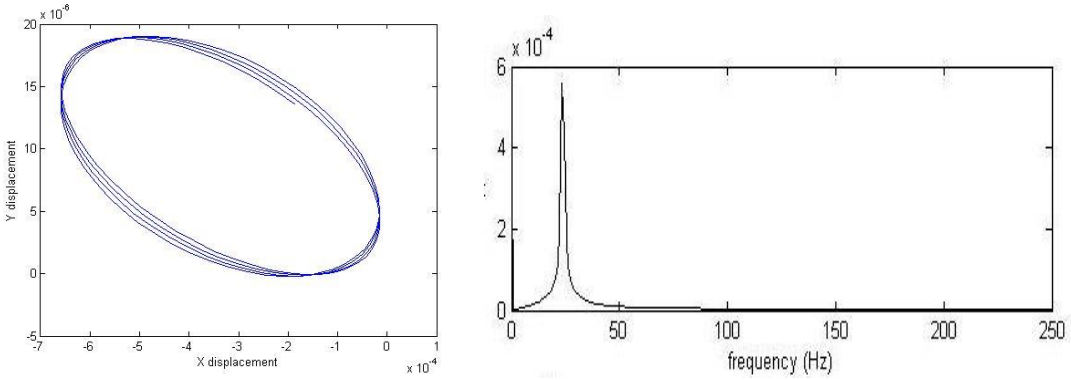

(a) Orbit plot (b) FFT curve in X direction

Figure 3-11 Dynamic response at 20000 rpm

Fig 3.12 presents the orbit plot and fft curve at 20600 rpm. At 20600 rpm the amplitude rises suddenly resulting in high vibration as can be seen from fig 3.12 (b). This is because of the nonlinear behavior of the foil bearing forces. As we know that foil bearing becomes more efficient with increasing speed and it was following that pattern as can be seen from the dynamic results till 20600 rpm. As this speed approaches the nonlinearities present in the bearing increases as a result the system becomes more unstable above this speed.

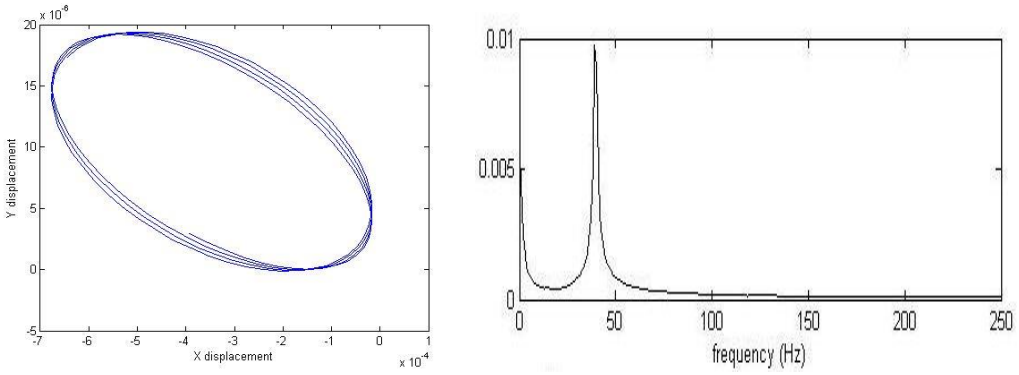

(a) Orbit plot (b) FFT curve in X direction

Figure 3-12 Dynamic response at 20600 rpm

3.3.1. Effect of bump pitch on response

Fig 3.13 depicts the effects of bump pitch on the dynamic response of the system. Fig 3.13(a) represents the response of a system at 10000 rpm with bump pitch value 4.572 mm. Fig 3.13(b) shows the response of the system with bump pitch 4.672 mm and similarly Fig3.13(c) represents response of system with bump pitch 3.772 mm. Only bump pitch value has been changed rest other parameters are kept constant. It can be seen that there are no signs of instability but with increasing bump pitch the amplitude is decreasing. The probable reason would be due to resulting higher damping with higher values of pitch.

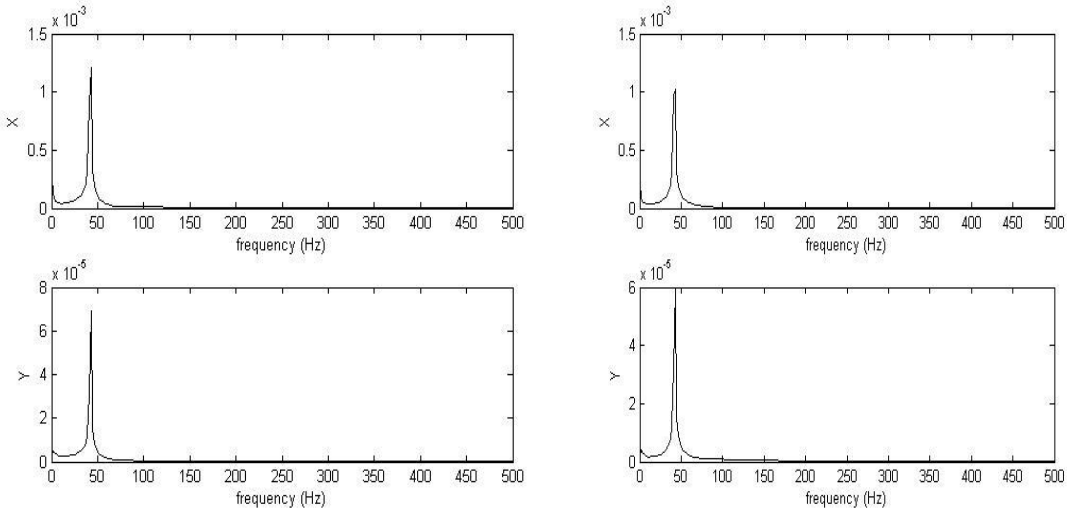

(a) FFT curve at s=4.572mm (b) FFT curve at s=4.672mm

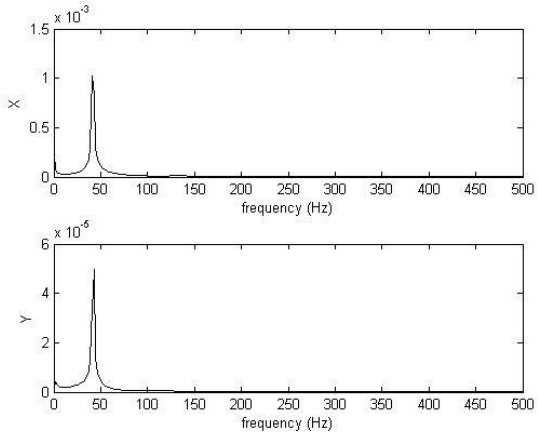

(c) FFT curve at s=4.772mm

Figure 3-13 Effect of bump pitch

3.3.2. Effect of foil thickness on the dynamic response of the system

Fig 3.14 shows the effect of the variation of bump foil thickness. Fig 3.14(a) represents the dynamic response of the rotor system at 10000 rpm with bump thickness value 0.108 mm. Similarly, Fig. 3.14 (b) and 3.14(c) represents the response of the rotor system with bump thickness 0.110 mm and 0.120 mm respectively. It can be inferred from the Fig. 3.14 that with the increasing bump thickness amplitude starts to increase. So thin bump should be used in the design.

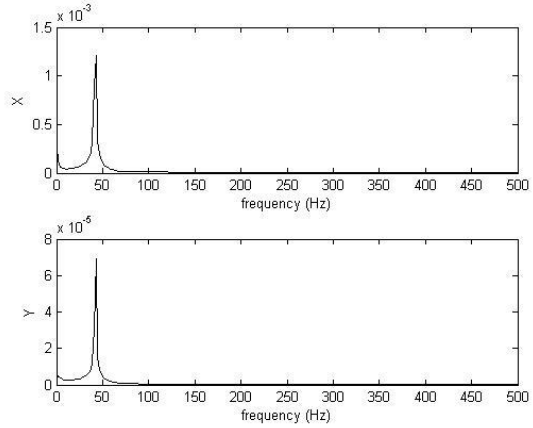

(a) FFT curve at t_b=0.102 mm

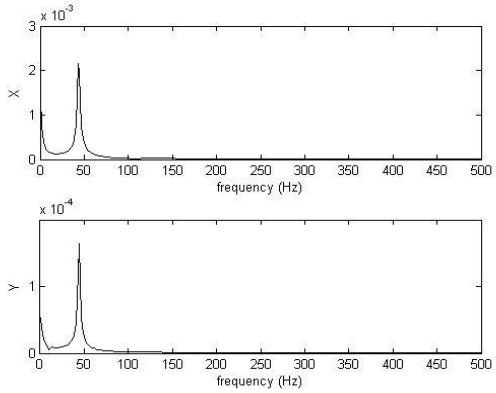

(b) FFT curve at t_b=0.110 mm

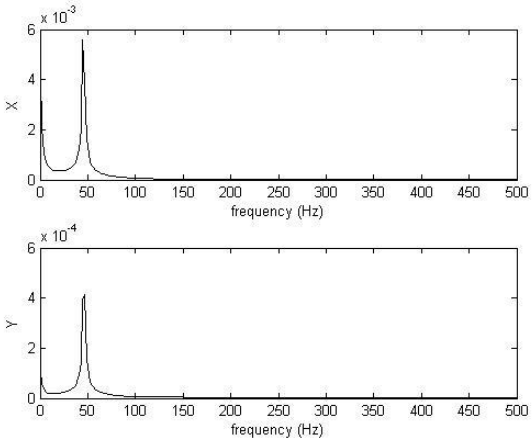

(c) FFT curve at t_b=0.120 mm

Figure 3-14 Effect of bump thickness

3.3.3. Effect of clearance on the dynamic response of the system

Fig 3.15 presents the effect of variation of clearance on the dynamic response of the rotor system. Fig 3.15(a) shows the dynamic response of the rotor system at 10000 rpm with clearance value 0.0318 mm. Similarly, Fig 3.15(b) and 3.15(c) represents the dynamic response of the system at C=0.0328 mm and C=0.0338 mm respectively. As it can be seen from the Fig 3.15 that initially with increase in clearance the amplitude increases but as the values are increased further it starts to decrease.

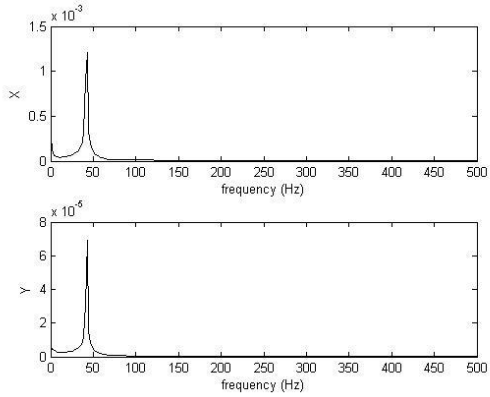

(a) FFT curve at C=0.0318 mm

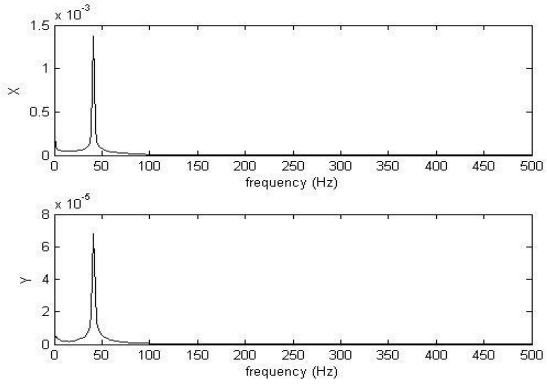

(b) FFT curve at C=0.0.0328 mm

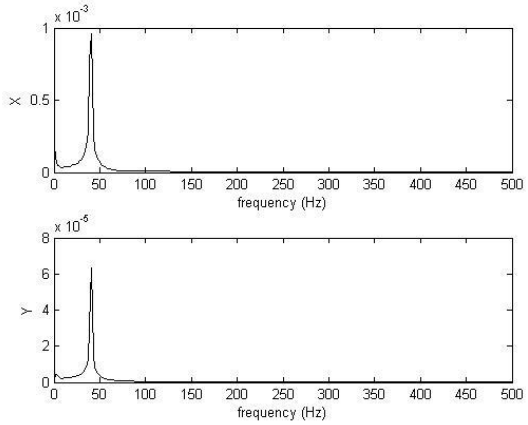

(c) FFT curve at C=0.0338 mm

Figure 3-15 Effect of clearance

From above parametric studies, it can be seen that the amplitude of response at the disc is a nonlinear function of bump foil thickness, bump pitch and clearance between the journal and the top foil. So, in order to design the foil bearing one can supply the response to a system so as to predict the optimum parameters of the bearing. For this neural network modeling is used.

3.4. **Neural Network Model**

A simple supervised neural network model consists of 3-layers Input, Output and hidden, each containing several nodes called neurons. Each layer neuron is connected to its adjacent layer neurons by weights. By providing inputs and target vectors one has to obtain a correct set of connection weights by means of training process which may take several cycles. In present work, the input layer consists of journal displacement amplitudes in X and Y directions and output layer consists of bearing parameters such as bump pitch, bump foil thickness and clearance. The training data is prepared by varying bump pitch, bump foil thickness and clearance, each in 5 levels and for each case a table of X, Y amplitudes are recorded. Inversely the data is trained with 2 inputs and 3 outputs. Neural network is implemented in Matlab tool box. The basic model is 3-layer feed forward back propagation network in which the number of hidden layer nodes is optimally selected for obtaining lowest possible error. In present work, a trail values of 4,5,……9 neurons are selected in the hidden layer. Fig. 3.16 shows the neural network configuration and Fig. 3.17 shows the training convergence trend for 100000 cycles.

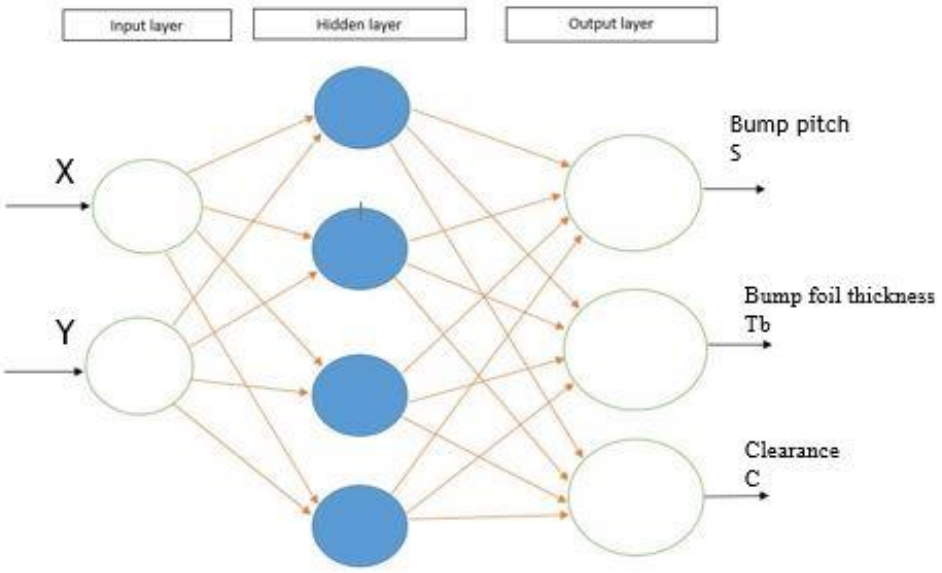

Figure 3-16 Neural Network Model

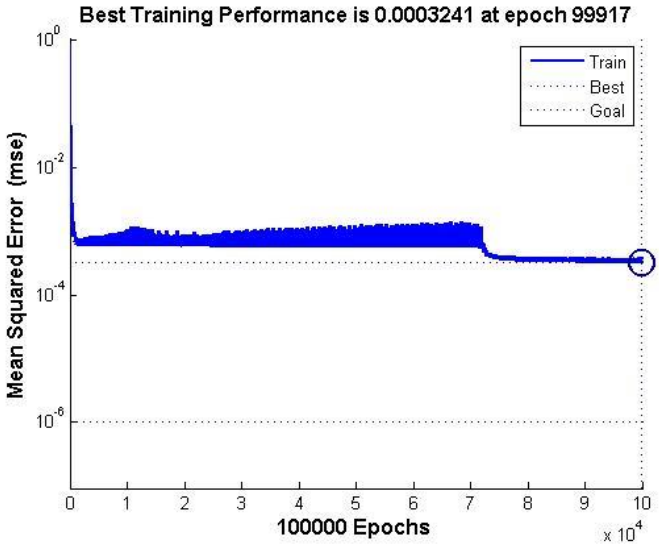

Figure 3-17 Mean square error

During the training log-log sigmoid function is used as an activation function to obtain the output. Fig. 3.18 shows the distribution of points around the true values during training. Total training samples are 100 and total testing samples are 25. After training and testing the neural network model can be used for finding the bearing parameters effectively from dynamic response.

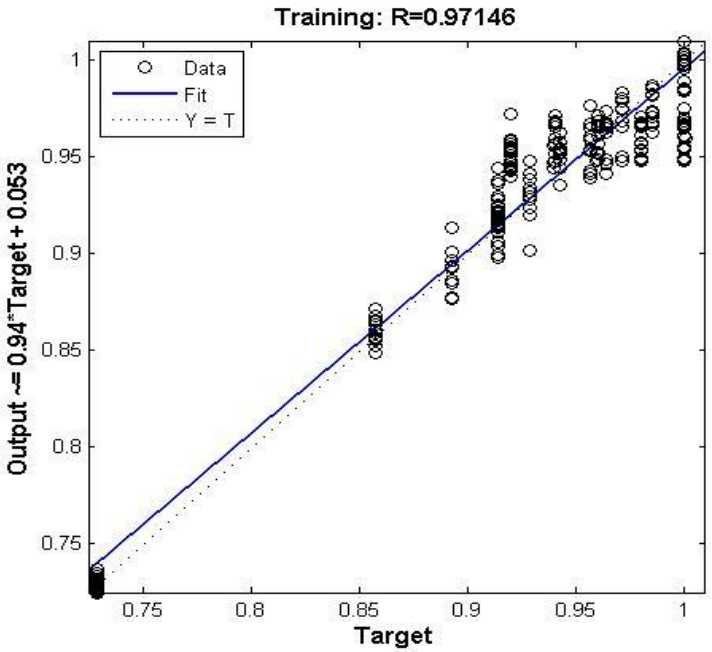

Figure 3-18 Training curve

For optimization of bearing parameters from dynamic response amplitudes we can use the process shown in Fig. 3.19.

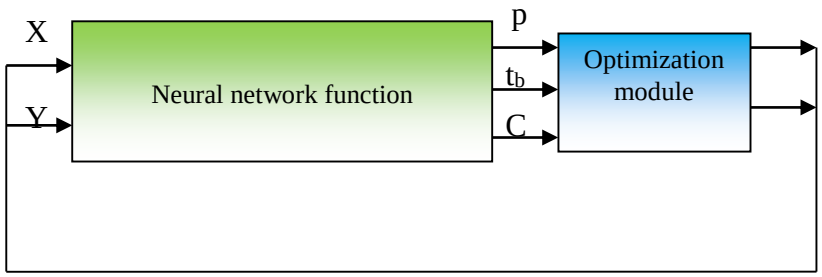

Figure 3-19 Optimum design process of foil bearing

Table 3.2 shows the identified values of the bearing parameters from neural network for unknown X Y values.

Table 3-4 Comparison of outputs from neural network

S. No.	Inputs		p		t_b		C	
	X	Y	NN	actual	NN	actual	NN	actual
1	0.0274	0.0036	0.00453	0.00467	$1.31e^{-4}$	$1.35e^{-4}$	$3.186e^{-5}$	$3.28e^{-5}$
2	0.0206	0.0031	$4.63e^{-3}$	$4.67e^{-3}$	$1.31e^{-4}$	$1.35e^{-4}$	$3.234e^{-5}$	$3.33e^{-5}$

3.5. Fabrication of scaled model

An attempt has been made here to fabricate the foil bearing rotor system. For fabrication purpose following steps has been followed:

3.5.1. Fabrication of the Disc

A disc of 12.7 cm diameter (5 inch) has been prepared via gas cutting and turning. The material of the disc prepared is steel. Fig. 3.20 shows the disc.

Figure 3-20 Steel Disc

3.5.2. Fabrication of shaft

For the purpose of fabrication of shaft, we have used a mild steel rod. The rod is turned to a diameter of 15 mm. Fig 3.21 shows the shaft.

Figure 3-21 Mild steel shaft

3.5.3. Fabrication of bump foil

The material used for the fabrication of bump foil is Aluminium. Firstly, a die is prepare with the required bump shape and then the aluminium foil is put over it and pressed mechanically to get the required shape on the foil.

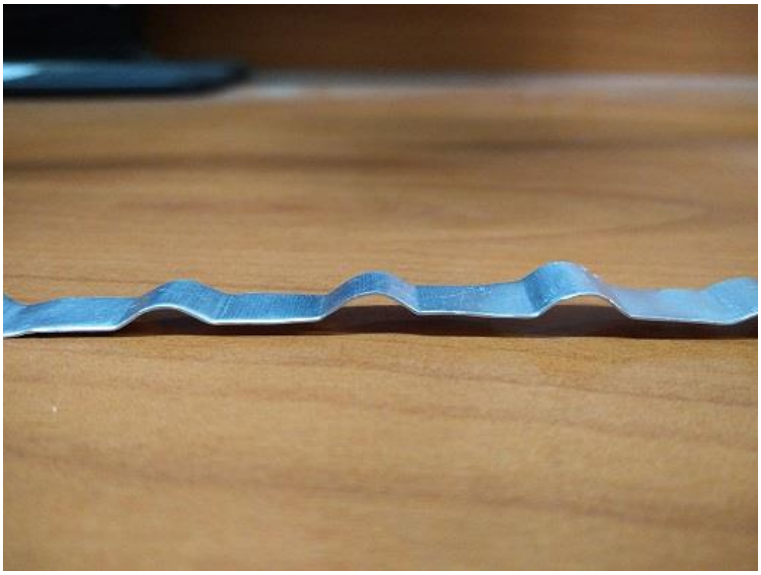

Figure 3-22 Bump foil

It is planned to conduct an experimental analysis on the rotor with at least one side having foil bearing. The other side of the shaft is supported on a SKF ball bearing. The disc is placed centrally. To construct foil bearing a hollow disc is selected along with another disc mounted on the shaft ends. The foil with bumps is carefully inserted in the space between the two discs so as to tightly fit in between without falling at higher speeds. The two bearings

are mounted on a wooden support pedestal having slots to mount the outer race/sleeve of the bearings. A simple modal analysis using vibration shaker and accelerometer has been planned to obtain first few natural frequencies of the system. The work is not completed.

Chapter 4

Conclusions and future work

In the present work, effects of gas foils bearing parameters on the dynamic response of a centrally mounted single disc shaft bearing system were studied. Initially the foil bearing forces were obtained from the pressure distribution and film thickness. These time varying forces were employed as bearing reactions in the single disc rotor dynamic analysis. The response was obtained by a lumped parameter model through the solution of differential equations. Effects of bump pitch, bump thickness and clearance between journal and top foil of the bearing on dynamic response at the disc mass were reported. A scaled model of the rotor bearing system was fabricated for testing its natural frequencies at laboratory.

4.1. Scope of future work

The present work is based on the computer program developed on Finite difference method for analysis of bearing forces. Depending on the type of bearing parameters, the dynamic characteristics such as natural frequencies and response amplitudes change. The present model of foil bearing forces is simple in nature and can be employed for any type of rotor bearing systems. The optimum dimensional parameters of the bearing are selected such that a maximum possible reduction of amplitudes is achieved with respect to rigid bearing supported rotor. For this some optimization schemes may be selected. Also, the scaled model with foil bearing needs some experimental test to find its natural frequencies using vibration shake and accelerometer along with oscilloscope and signal generator. Even this model is not new it given an exercise of implementing several numerical methods for dynamic analysis. Finally, the 3-D model of the rotor bearing system must be improvised to take care of several nonlinear effects.

References

1. F.Balducchi, M.Arghir, R.Gauthier, Eexperimental ‘Analysis of the unbalance response of the rigid rotors supported on aerodynamic foil bearings’, Journal of vibration and acoustics, Vol. 137, pp. 061014-1 to 11, 2015

2. Jon S. Larsen, Ilmar F. Santos, ‘On the nonlinear steady-state response of rigid rotors supported by air foil bearings—Theory and experiments’, journal of sound and vibration, Vol. 346, pp-284-297, 2015

3. J.S.Larsen, A.C.Varela, I.F.Santos, ‘Numerical and experimental investigation of bump foil mechanical behavior’, Tribology International, Vol. 74, pp-46-56,2014

4. P.Bonello, H. M. Pham, ‘The efficient computation of the nonlinear dynamic response of a foil–air bearing rotor system’, Journal of sound and vibration, Vol. 333, pp. 3459-3478, 2014

5. Li-Hua Yang, Wei-Min Wang, Shi-Quan Zhao, Yan-Hua Sun, Lie Yu, ‘A new nonlinear dynamic analysis method of rotor system supported by oil film journal bearings’, Applied mathematical modelling, Vol. 38, pp. 5239-5255, 2014

6. M.H. Jalali, M. Ghayour, Saeed Ziaei-Rad, B. Shahriari, ‘Dynamic analysis of a high speed rotor bearing system’, Measurement, Vol. 53, pp. 1-9, 2014

7. P.Bhore , A.K. Darpe, ‘Nonlinear dynamics of flexible rotor supported on the gas foil journal bearings’, Journal of sound and vibration, Vol. 332, pp-5135-5150, 2013

8. N. Biswas, Sk. Hikmat, R. Tiwari, ‘Transient analysis of a 3 lobe bearing at 80000 rpm for a gas turbine’, International of recent advances in mechanical engineering, Vol.2, No. 1, 2013

9. H. Yu, C. Shuantao, C. Rugang, Z. Qiaoyu, Z. Hongli, ‘Numerical study on foil journal bearings with protuberant foil structure’, Tribology International, Vol. 44, pp. 1061-1070, 2011

10. R.G. Chen, Q. Zhao, Y. Liu, Y. Hou, ‘A preliminary study of the load bearing capacity of a new foil thrust gas bearing’, Journal of Mechanical Engineering Science, Vol. 225, pp-673-678, 2011

11. M. Kumar, D. Kim, ‘Static performance of hydrostatic air bump foil bearing’, Tribology International, Vol. 43, pp. 752-758, 2010

12. D.H. Lee, Y.C. Kim, H.W. Kim, ‘The effect of coulomb friction on the static performance of foil journal bearing’, Tribology International, Vol. 43, pp. 1065-1072, 2010

13. Arora V., Hoogt P. J. M. van der, Aarts R.G.K.M., De Boer A.Der, (2010), ‘Identification of dynamic properties of radial air-foil bearings’, International journal of mechancis and materials in design, Vol. 6, Issue 4, pp-305-318, 2010

14. D.H. Lee, Y.C. Kim, K.W. Kim, ‘The dynamic performance analysis of foil journal bearings considering coulomb friction: Rotating Unbalance Response’, Tribology Transactions, Vol. 52:2, pp. 146-156, 2009

15. Daejong Kim, Soongook Park, ‘Hydrostatic air foil bearings: Analytical and experimental investigation’, Tribology International, Vol. 42, pp- 413-425, 2009

16. I. Iordanoff, B. Bou Said, A. Mezianne, Y. Berthier, ‘Effect of internal friction in the dynamic behaviour of aerodynamic foil bearings’, Tribology International, Vol. 41, pp- 387-395, 2008

17. Luis San Andres, Tae Ho Kim, ‘Forced nonlinear response of gas foil bearing supported rotors’, Tribology International, Vol. 41, pp-704-715, 2008

18. Yong-Bok Lee, Tae-Ho Kim, Chang-Ho Kim, Nam-Soo Lee, Dong-Hoon Choi, ‘Dynamic characteristics of a flexible rotor system supported by a viscoelastic foil bearing (VEFB)’, Tribology International, Vol. 37, pp- 679-687, 2004

19. Howard Samuel A., Dykas Brian, “Journal Design Considerations for Turbomachine Shafts Supported on Foil Air Bearings”, Tribology Transactions, 47: 508-516, 2004

20. Dellacorte C., Valco M. J., “Load Capacity Estimation of Foil Air Journal Bearings for Oil-Free Turbomachinery Applications”, Tribology Transactions, 43: 795-801, 2000

APPENDIX I

Computer program for finding foil bearing forces

```
clc
clear all
%input to the program
ntheta=61;  % no of grids in theta direction
nz=61;      % no of grids in z direction
% INPUTS
C=0.0318e-3;       % radial clearance
R=19.05e-3;         % radius of shaft
L=38.1e-3;         % length of bearing
s=4.572e-3;       % bump pitch
pat=0.1e6;      % atmospheric pressure
l=1.778e-3;      % half bump length
tb=0.102e-3;        % thickness of bump foil
v=0.29;       % poisson's ratio
nu=1.786e-5;  % viscocity of lubricant
delphi=0.0477;
speed=10000;  % rpm
w=(2*pi*speed)/60;% angular speed of rotation
er=0.8;
%Xb=0.7;
%Yb=0.31;
Et=214e9;   % modulus of elasticity of bump foil
lambda=(6*nu*w/pat)*((R/C)^2);
%lambda=10;
alpha= (2*pat*s/(C*Et))*((l/tb)^3)*(1-(v^2)); %compliance no.

z=linspace(0,L,nz);%Generation of row matrix having equally spaced 100
elements between ri & ro
Theta=linspace(0,2*pi,ntheta);%Generation of row matrix having equally
spaced 100 elements between 0 & 2*pi
[THETA,Z]=meshgrid(Theta,z);    % generation of 100*100 matrix
corresponding to each THETA & R
zz=Z/C;

hr=ones(size(THETA));
for  j=1:ntheta
    for i=1:nz
        %hr(i,j)=1+Xb*cos(THETA(i,j))+Yb*sin(THETA(i,j));
        hr(i,j)=1+er*cos(THETA(i,j));
    end
end
surf(hr)
%% Find the pressure in while loop till it converge, for air bearing
newton rapsom method can be used to solve the qudratic equation
P=ones(size(THETA));  %p=Atmospheric pressure
p=(P.*P);
H=hr;%converting in nondimensional form
deltath=(2*pi)/(ntheta-1);%defining the deltatheta
deltazb=((L-0)/R)/(nz-1);%defining the deltarb
%Pn=1;
ITER=1000;
for I=1:ITER
    sumij=0.0;
    for i=2:nz-1
        for j=2:ntheta-1
            %delta(i,j)=alpha*(sqrt(p(i,j)-1));
```

```
            %H(i,j)=hr(i,j)+delta(i,j);
            H1=(H(i+1,j)+H(i,j))/2;
            H2=(H(i,j)+H(i-1,j))/2;
            H3=(H(i,j+1)+H(i,j))/2;
            H4=(H(i,j)+H(i,j-1))/2;

k=((((H3)^3+(H4)^3))/(deltath^2))+((2*(H(i,j))^3)/(deltazb^2));
            k1=((H(i,j))^3)/(deltazb^2);
            k2=((H(i,j))^3)/(deltazb^2);
            k3=(((H3)^3)/(deltath^2));
            k4=(((H4)^3)/(deltath^2));
            k5=-((lambda/(deltath))*H(i,j+1));
            k6=((lambda/(deltath))*H(i,j-1));
            p(i,j)=((k1/k)*(p(i+1,j)))+((k2/k)*(p(i-
1,j)))+((k3/k)*(p(i,j+1)))+((k4/k)*(p(i,j-
1)))+((k5/k)*(sqrt(p(i,j+1))))+((k6/k)*(sqrt(p(i,j-1))));
            if p(i,j)<1
                p(i,j)=1;
            end
            sumij=sumij+p(i,j);
        end
    end
        sum1(I+1)=sumij;
        percentage=abs(sum1(I+1)-sum1(I))/abs(sum1(I+1));
        if percentage<0.0001
            break;
        end
Y=I;
Pact=sqrt(p);

delta1=alpha*(Pact-ones(size(Pact)));
hb=hr+delta1;
plot(THETA,Pact)

end
```

end

```
num=61;
    gx=Pact.*cos(THETA);
    gy=Pact.*sin(THETA);
    sc=2*ones(num,1);
    sc(2:2:num-1)=4;
    sc(1)=1;
    sc(num)=1;
    scx=meshgrid(sc,sc);
    scxy=ones(num,num);
    scxy(2:2:num-1,:)=scx(2:2:num-1,:)*sc(2);
    scxy(3:2:num-2,:)=scx(3:2:num-2,:)*sc(3);
    scxy(1,:)=sc';
    scxy(num,:)=sc';
    hx=deltath;
    hy=deltazb;
    h=(hx*hy)/9;
    fx=-h*sum(sum(scxy.*gx));
    fy=-h*sum(sum(scxy.*gy));
    W=sqrt(fx^2+fy^2);
```